Astroparticle Physics 63 (2015) 23–41

Contents lists available at ScienceDirect

Astroparticle Physics

journal homepage: www.elsevier.com/locate/astropart

Growth of cosmic structure: Probing dark energy beyond expansion

Dragan Huterer [a,*], David Kirkby [b], Rachel Bean [c], Andrew Connolly [d], Kyle Dawson [e], Scott Dodelson [f,g], August Evrard [a], Bhuvnesh Jain [h], Michael Jarvis [h], Eric Linder [i], Rachel Mandelbaum [j], Morgan May [k], Alvise Raccanelli [l], Beth Reid [i], Eduardo Rozo [m], Fabian Schmidt [n,q], Neelima Sehgal [o], Anže Slosar [k], Alex van Engelen [o], Hao-Yi Wu [a], Gongbo Zhao [p]

[a] Department of Physics, University of Michigan, 450 Church St, Ann Arbor, MI 48109-1040, USA
[b] Department of Physics and Astronomy, UC Irvine, 4129 Frederick Reines Hall, Irvine, CA 92697-4575, USA
[c] Department of Astronomy, Cornell University, Ithaca, NY 14853, USA
[d] Department of Astronomy, University of Washington, Seattle, WA, USA
[e] Department of Physics & Astronomy, University of Utah, 115 South 1400 East #201, Salt Lake City, UT 84112, USA
[f] Fermilab Center for Particle Astrophysics, Fermi National Accelerator Laboratory, Batavia, IL 60510-0500, USA
[g] Department of Astronomy & Astrophysics, University of Chicago, Chicago, IL 60637, USA
[h] Department of Physics and Astronomy, University of Pennsylvania, 209 South 33rd Street, Philadelphia, PA 19104, USA
[i] Physics Division, Lawrence Berkeley National Laboratory, 1 Cyclotron Road, Berkeley, CA 94720, USA
[j] Department of Physics, Carnegie Mellon University, Pittsburgh, PA 15213, USA
[k] Brookhaven National Laboratory, Upton, NY 11973, USA
[l] NASA Jet Propulsion Laboratory, California Institute of Technology, Pasadena, CA 91109, USA
[m] SLAC National Accelerator Laboratory, Menlo Park, CA 94025, USA
[n] Department of Astrophysical Sciences, Princeton University, Princeton, NJ 08544, USA
[o] Stony Brook University, Stony Brook, NY 11794, USA
[p] National Astronomy Observatories, Chinese Academy of Science, Beijing 100012, PR China
[q] Max-Planck-Insitute for Astrophysics, D-85748 Garching, Germany

ARTICLE INFO

Article history:
Received 30 October 2013
Received in revised form 20 June 2014
Accepted 3 July 2014
Available online 11 July 2014

Keywords:
Cosmology
Large-scale structure
Dark energy

ABSTRACT

The quantity and quality of cosmic structure observations have greatly accelerated in recent years, and further leaps forward will be facilitated by imminent projects. These will enable us to map the evolution of dark and baryonic matter density fluctuations over cosmic history. The way that these fluctuations vary over space and time is sensitive to several pieces of fundamental physics: the primordial perturbations generated by GUT-scale physics; neutrino masses and interactions; the nature of dark matter and dark energy. We focus on the last of these here: the ways that combining probes of growth with those of the cosmic expansion such as distance-redshift relations will pin down the mechanism driving the acceleration of the Universe.

One way to explain the acceleration of the Universe is invoke dark energy parameterized by an equation of state w. Distance measurements provide one set of constraints on w, but dark energy also affects how rapidly structure grows; the greater the acceleration, the more suppressed the growth of structure. Upcoming surveys are therefore designed to probe w with direct observations of the distance scale and the growth of structure, each complementing the other on systematic errors and constraints on dark energy. A consistent set of results will greatly increase the reliability of the final answer.

Another possibility is that there is no dark energy, but that General Relativity does not describe the laws of physics accurately on large scales. While the properties of gravity have been measured with exquisite precision at stellar system scales and densities, within our solar system and by binary pulsar systems, its properties in different environments are poorly constrained. To fully understand if General Relativity is the complete theory of gravity we must test gravity across a spectrum of scales and densities. Rapid developments in gravitational wave astronomy and numerical relativity are directed at testing gravity in the high curvature, high density regime. Cosmological evolution provides a polar opposite test bed, probing how gravity behaves in the lowest curvature, low density environments.

There are a number of different implementations of astrophysically relevant modifications of gravity. Generically, the models are able to reproduce the distance measurements while at the same time altering the growth of structure. In particular, as detailed below, the Poisson equation relating over-densities to

* Corresponding author. Tel.: +1 734 615 3289.
E-mail address: huterer@umich.edu (D. Huterer).

http://dx.doi.org/10.1016/j.astropartphys.2014.07.004
0927-6505/

gravitational potentials is altered, and the potential that determines the geodesics of relativistic particles (such as photons) differs from the potential that determines the motion of non-relativistic particles. Upcoming surveys will exploit these differences to determine whether the acceleration of the Universe is due to dark energy or to modified gravity.

To realize this potential, both wide field imaging and spectroscopic redshift surveys play crucial roles. Projects including DES, eBOSS, DESI, PFS, LSST, *Euclid*, and *WFIRST* are in line to map more than a 1000 cubic-billion-light-year volume of the Universe. These will map the cosmic structure growth rate to 1% in the redshift range $0 < z < 2$, over the last 3/4 of the age of the Universe.

1. Introduction: why measuring growth is interesting

The standard cosmological model posits that the largest structures that we observe today – galaxies and clusters of galaxies – grew out of small initial fluctuations that were seeded during the phase of inflationary expansion, some 10^{-35} s after the Big Bang. Subsequently these fluctuations grew under the influence of gravity. Most of the growth occurred after the decoupling of photons and electrons, some 350,000 years after the Big Bang, when photons cease to be coupled to baryons and provide pressure support against gravitational collapse. The Jeans mass – smallest mass that can undergo gravitational collapse – therefore drastically drops at decoupling. This, as well as the fact that the Universe was mostly matter-dominated at that point, allows the galactic-size structures to grow unimpeded.

In the currently favored cosmological model, where most of the matter budget is dominated by the slow-moving massive particles (the "cold dark matter" or CDM), the smaller structures form first, while the largest structures form the latest. Therefore, objects that are of the most interest to cosmologists, galaxies and clusters of galaxies, form at recent times and, in some cases, are still forming today. Hence, observations in various wavelengths can probe the full evolution of the formation of structure in the Universe, from when the first objects formed until today.

Observations of the growth of structure provide a wealth of information about dark matter and dark energy. In particular, the scaling of the amplitude of growth vs. cosmic time – the so-called growth function – sensitively constrains dark energy parameters in a way that is complementary to distance measurements. The temporal evolution of the growth is now readily observed by measuring the clustering of galaxies at multiple redshifts, and in the near future gravitational lensing has the potential to measure the same quantity but with the added advantage that it is directly sensitive to the growth of dark matter structures (as opposed to galaxies or other baryonic tracers such as hydrogen in the inter-galactic medium). Additionally, the number counts of clusters of galaxies, as a function of their mass and redshift, provide another excellent probe of cosmological parameters. Our ability to observe and model both the growth and the cluster counts have significantly matured over the past decade, and these two probes now provide constraints on dark energy that are complementary to distance measurements by type Ia supernovae, baryon acoustic oscillations (BAO; which encode geometrical aspects of the clustering of galaxies), and the cosmic microwave background (CMB).

Over the next 10–20 years, we expect a wealth of new observations that include ground imaging surveys (e.g. DES and LSST), redshift surveys (e.g. eBOSS, PFS and DESI) and space surveys (e.g. *Euclid* and *WFIRST*). The combination of these observations will provide high-precision measurements of the growth of structure out to redshift of a few and across most of the sky. These measurements will, in turn, strongly constrain the equation of state of dark energy and, more generally, the expansion history of the Universe (discussed in the Snowmass-2013 paper on Distances [1]) over the past ~10 billion years.

The growth of structure is particularly sensitive as a probe of modified-gravity explanations for the accelerating Universe, and has already been used to impose constraints on the extensions of, and modifications to, General Relativity (GR). The effectiveness of the growth of structure in this regard is maximized when it is combined with distance measurements, which can be understood as follows. Modified-gravity models are constructed so that they reproduce distances consistent with their current measurements which, in the context of GR, indicate an accelerating universe. Importantly, these models generally predict the growth-of-structure history that is different from the GR prediction given those same distance measurements. Therefore, independent precision measurements of the growth of structure test whether GR adequately describes the late-time expansion of the Universe. Such tests are paramount to our understanding of dark energy and may lead to fundamental discoveries of physics at large scales, and this makes the growth of structure a very important probe of the Universe.

Good complementarity, redundancy, and control of the systematic errors are keys in making the growth of structure observations reach their full potential. Photometric and spectroscopic surveys are particularly complementary in various aspects of their observational strategies; moreover, spectroscopic surveys play an additional key role of calibrating the photometric redshifts obtained from galaxy colors. Multiple observations of the same sky coverage may be useful for this reason, while non-overlapping observations help reduce cosmic variance. Finally, numerical (N-body) simulations have an extremely important role of providing theoretical predictions for the growth of structure in the quasi-linear regime (roughly 10–50 megaparsecs) and especially in the non-linear regime (scales less than about 10 megaparsecs).

The paper is organized in follows. In Section 2 we define what precisely we mean by the growth of structure, and broadly illustrate constraints on it from future surveys. In Section 3 we discuss how the growth of structure probes the dark-energy and modified-gravity explanations for the acceleration of the Universe. In Section 4 we discuss in some detail several of the most promising probes of the growth of structure – clustering of galaxies in spectroscopic surveys, counts of galaxy clusters, and weak gravitational lensing. Finally in Section 5 we discuss the very important role of simulations in theoretically predicting growth on non-linear scales.

2. Preliminaries and definitions

In the linear theory – valid at sufficiently early times and sufficiently large spatial scales, when the fluctuations in the matter energy density ρ_M are much less than unity – the matter density contrast $\delta(t) = \delta\rho_M/\rho_M$ evolves independently of the spatial scale k. The growth of fluctuations in time (well within the Hubble radius) $\delta(t)$ can be obtained by solving the equation

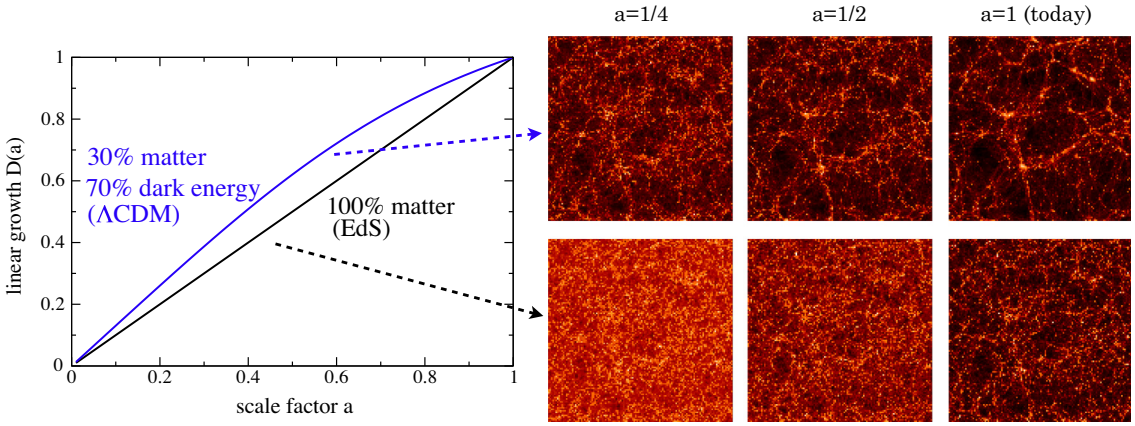

Fig. 1. Growth of structure at large spatial scales in the universe. *Left panel:* Because dark energy suppresses the growth of structure, the linear growth $D(a)$, which is normalized to unity today, had to be larger in the past in the currently favored model with dark energy (ΛCDM; blue line) than in the Einstein–de Sitter model (EdS; black line) which has matter only and no dark energy. *Right panel:* snapshots from numerical (N-body) simulations by the Virgo consortium [2], showing larger amplitude of density fluctuations in the past in ΛCDM (top row) than in the EdS model (bottom row) given an approximately fixed amount of clustering today. Accurate measurements of the clustering as a function of spatial scale and cosmic time can therefore stringently constrain the cosmological model. (For interpretation of the references to color in this figure legend, the reader is referred to the web version of this article.)

$$\ddot{\delta} + 2H\dot{\delta} - 4\pi G\rho_M\delta = 0, \tag{1}$$

where $H(t)$ is the Hubble parameter, $\rho_M(t)$ is the matter energy density, and dots are derivatives with respect to time t. Therefore, in standard General Relativity and in the linear regime ($|\delta| \ll 1$), obtaining the linear growth of fluctuations as a function of time is straightforward given the composition and the expansion rate of the Universe. More commonly, one works in terms of the scale factor a, where $d\ln a = Hdt$, and $a = 0$ ($a = 1$) at the Big Bang (today). One can then define the *linear growth function* $D(a)$ via

$$\delta(a) = D(a)\delta(a = 1) \tag{2}$$

or equivalently in redshift z where $1 + z = 1/a$. If General Relativity is replaced by some modified gravity theory, then Eq. (1) changes: the evolution of growth needs to be re-derived in the new theory, and the linear growth rate D may then depend on scale k as well. The left panel of Fig. 1 illustrates the linear growth function for two representative cosmological models, and the right panel provides snapshots from numerical simulation further illustrating the suppressed growth of structure in the presence of dark energy.

It is useful to make a connection to other quantities commonly used to probe growth. First of all, we can define the matter *power spectrum* $P(k)$ as the Fourier transform of the 2-point correlation function, $\langle\delta_{\vec{k}}\delta^*_{\vec{k}'}\rangle = (2\pi)^3\delta^{(3)}(\vec{k} - \vec{k}')\,P(k)$. Note that $P(\vec{k}) = P(k)$ due to isotropy of the Universe and the scale-factor- (or redshift-) dependence of both δ and P is implicit. A commonly used quantity is the rms *amplitude of mass fluctuations*, whose square (i.e. the variance of mass fluctuations σ_R^2) is given by the integral over the power spectrum defined *in linear theory*

$$\sigma_R^2(a) = \int_0^\infty \frac{k^3 P_{\rm linear}(k,a)}{2\pi^2}\,W^2(kR)\,d\ln k, \tag{3}$$

where $W(x) = 3j_1(x)/x$ is the Fourier transform of the real-space window function. The quantity $\sigma_R(a)$ encodes the amount of matter fluctuations averaged over a sphere of radius R at redshift z, assuming that the fluctuations are fully linear (thus Eq. (1) is valid). A common choice to describe the normalization of the fluctuations in the Universe *today* is $\sigma_8 \equiv \sigma_{8\ h^{-1}\ \rm Mpc}(a = 1)$. Measurements of the redshift-dependence of σ_8 are sometimes quoted as probes of the growth function $D(a)$, since $\sigma_8(a) = \sigma_8 D(a)$.

Fig. 2 shows an example of constraints from the growth of structure, shown for only one of the cosmological probes – the redshift-space distortions (RSD), which will be further discussed in Section 4.1. This probe is sensitive to the derivative of the logarithm of the growth function with respect to logarithm of the cosmic scale[1]; we thus show the quantity

$$f(a) \equiv \frac{d\ln D}{d\ln a} \tag{4}$$

vs. the redshift $z \equiv 1/a - 1$. We show theory predictions for the currently favored cosmological constant plus cold dark matter (ΛCDM) model, as well as for two modified-gravity models, the Dvali–Gabadadze–Porrati braneworld model (DGP; [3]), and the $f(R)$ modification to Einstein action from Ref. [4] with $c = 3$. Because growth in the $f(R)$ models is generically scale-dependent, we show predictions at two wavenumbers, $k = 0.02$ h Mpc^{-1} and $k = 0.1$ h Mpc^{-1}. The $f(R)$ model – which is usually challenging to distinguish from GR because it can have the expansion history mimicking the ΛCDM model (w is within 1% of -1) and can have a growth function identical to Λ's at high redshift – can clearly be distinguished from ΛCDM using growth data from future surveys such as eBOSS, DESI, *Euclid*, or *WFIRST*. The DGP model can be distinguished even more readily by measuring both the expansion history as well as growth of structure in the Universe.

3. Dark energy and modified gravity

Over the past decade, the ΛCDM paradigm has passed all observational tests, firmly establishing it as our cosmological "standard model". However, it is clearly of crucial importance to test this paradigm, given that it involves two unknown ingredients (dark matter and Λ), and given the lack of theoretical motivation for the value of the putative cosmological constant. Growth of structure offers a broad range of probes of dark energy which in principle cover three orders of magnitude in length scale, and one order of magnitude in time or scale factor. In order to convincingly rule out alternatives to the cosmological constant, we need to cover this range of scales and redshifts. Large-scale structure also provides model-independent tests of gravity on Mpc scales and above, extending Solar System tests by ten orders of magnitude in length scale.

In this section we briefly discuss the theoretical underpinnings of the tests of the accelerating Universe with the growth of cosmic structure. Modified gravity in particular is covered in much more

[1] More precisely, the RSD are sensitive to $\sigma_8(a)$ times this quantity, but we ignore this subtle distinction for the moment.

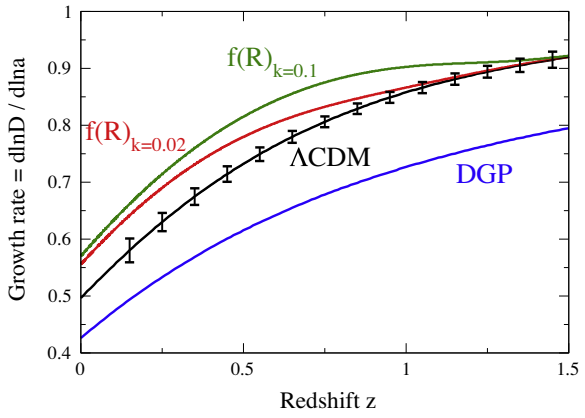

Fig. 2. Constraints on the growth of density fluctuations in the Universe with errors projected from a future survey designed with DESI specifications. The curves show the derivative of the logarithmic growth with respect to the logarithmic scale factor – a quantity readily measured from the clustering of galaxies in redshift space – as a function of redshift. We show theory predictions for the ΛCDM model, as well as for two modified-gravity models: the Dvali–Gabadadze–Porrati braneworld model [3] and the $f(R)$ modification to the Einstein action [4]. Because growth in the $f(R)$ models is generically scale-dependent, we show predictions at two wavenumbers, $k = 0.02$ h Mpc^{-1} and $k = 0.1$ h Mpc^{-1}. LSST projects to impose constraints of similar excellent quality on the growth function $D(a)$.

detail in the Snowmass-2013 paper on Novel Probes of Gravity and Dark Energy [5].

3.1. Dark energy

The physics behind the observed accelerated expansion of the Universe is widely recognized as one of the most profound outstanding problems in fundamental science. When interpreted in terms of our current understanding of gravity, Einstein's General Relativity, this requires adding an additional, exotic component to the cosmic energy budget with a negative pressure, which we now refer to as "dark energy".

The minimalist explanation is to invoke a very small cosmological constant. However, within our current understanding of quantum theory, such a value of the cosmological constant is extremely unnatural. Instead, one can invoke a very light scalar field, whose potential energy then drives the accelerated expansion of the Universe (this of course does not solve the cosmological constant problem). In fact, this is precisely the mechanism that presumably produced inflation, an epoch of extremely rapid expansion in the very early Universe which allowed the Universe to grow to its observed large size, and which provided the seed fluctuations for the structure within the Universe. While we have no good theoretical framework to connect the very early and late time epochs of acceleration, inflation can be seen as a tantalizing hint that the late time acceleration might be transitory and thus not be due to a cosmological constant. Observationally, we can distinguish this case by measuring the equation of state parameter $w \equiv p_{\rm DE}/\rho_{\rm DE}$, which is exactly -1 for a cosmological constant but slightly larger for a "slowly rolling" scalar field. The parameter w affects both the expansion history (geometry) of the Universe as well as the growth of structure within it.

A smooth dark energy component is completely described by its equation of state as function of time, $w(t)$. For this reason, *there is a consistency relation between the expansion history (for example, as measured by type Ia supernovae or BAO) and the growth of structure as measured by weak lensing, galaxy clusters, and redshift space distortions*. In simplest terms, this can be illustrated as the consistency between the linear perturbations $\delta(t)$ and the expansion history determined via the Hubble parameter $H(t)$ – in standard, unmodified GR, they need to satisfy the linear growth equation (Eq. (1)). Thus, measurements of the large-scale structure can unambiguously falsify the smooth dark energy paradigm.

Going beyond the simplest models of dark energy, one can consider fluctuations in the dark energy density, which require (at least at some point in time) a value of w significantly different from -1. The amplitude of these fluctuations is controlled by the sound speed of the scalar degree of freedom. Further, one can allow for a coupling of the scalar field to other components of matter. While a coupling to ordinary matter and radiation is constrained to be small (but see below), a coupling to dark matter is much less constrained and can only be probed through large-scale structure. These possibilities go beyond the simplest models of dark energy; however, they are still allowed by the data and, if detected, would allow for rich insights into the physics of dark energy and dark matter.

3.2. Modified gravity

As a fundamental alternative to dark energy, one can ask whether the acceleration of the Universe is caused by a modification of gravity on large scales, i.e. departure from GR, rather than an exotic form of energy. This possibility has generated a significant amount of theoretical work over the past decade; it furthermore provides strong motivation to search for and constrain modifications to GR using cosmological observations. However, modifying GR on large scales in a consistent way is extremely difficult, due to both theoretical issues and a broad set of observational constraints. In particular, any theory of gravity has to reduce to GR within the Solar System to satisfy stringent local tests of gravity. Further, the cosmic microwave background and the Big Bang nucleosynthesis provide constraints in the early Universe. Both of these constraints can be satisfied by invoking non-linear "screening mechanisms" which restore GR in high density regions.

Several mechanisms that achieve this have been proposed in the literature; they manage to hide a light scalar degree of freedom with gravitational-strength coupling to matter in high density regions. They operate by either making the field massive in high-density regions (chameleon mechanism), or suppressing its coupling through non-linear interactions (Vainshtein and symmetron mechanisms). When placing constraints on gravity models using structure in the non-linear regime it is then important to take into account the effects of these screening mechanisms. For example, in models with chameleon screening, the abundance of massive halos is not strongly enhanced over ΛCDM as predictions from linear growth of structure would suggest. On the other hand, the screening mechanisms can lead to unique signatures of their own in large-scale structure. These screening mechanisms are also relevant for models with a dark energy coupled to ordinary matter.

3.3. Distinguishing between dark energy and modified gravity

In order to distinguish between a smooth dark energy component and less minimal models such as coupled dark energy or modified gravity, it is crucial to measure the growth of structure in addition to the expansion history. This is because any given expansion history predicted by a modified gravity model could be emulated by a smooth dark energy component.

Observations of the large-scale structure can roughly be divided into two regimes:

- On *large scales*, fractional density perturbations are much less than one and are amenable to a perturbative treatment, so that the theoretical predictions for the growth are very accurate. In the context of dark energy and modified gravity, this regime is useful since one can parametrize the stress-energy content

of the Universe as well as the relation between stress energy and metric potentials, that is, gravity. Thus, in this regime one can place model-independent constraints on general dark energy models and modifications to gravity.

- On *smaller scales* ($\lesssim 10$ Mpc), density fluctuations become non-linear, and the perturbative treatment breaks down. Nevertheless, on scales larger than a few Mpc gravity is still the only relevant force, and quantitative predictions can be made through *N*-body simulations which are discussed in Section 5. Thus, this regime can still be used to probe gravity and dark energy. While clearly much more challenging to model and confront with data, the bulk of the information delivered by growth is in this regime, so it is essential to make use of it. In case of modifications to gravity, it is important to take into account the screening mechanisms as well.

Large-scale structure surveys provide a broad set of observables for this purpose (see Fig. 3). The abundance, clustering, and motions of large-scale structure tracers, such as galaxies, clusters, and the intergalactic medium, can be measured through a variety of methods, such as photometric and spectroscopic galaxy surveys, X-ray surveys, and small-scale CMB observations (see Section 4.2). Furthermore, the velocities of tracers such as galaxies can be inferred from their Doppler shifts, which in turn probe the (non-relativistic) cosmic potential wells. A fundamentally different observable is gravitational lensing, measured through the distortions induced in shapes of background galaxies (Section 4.3). The crucial property of gravitational lensing is that it probes all matter, whether dark or baryonic. Furthermore, lensing is governed by a spacetime perturbation different from the perturbation that determines the motion of non-relativistic bodies such as galaxies. By comparing velocities (dynamics) with lensing, one can perform a targeted, model-independent test of gravity which is largely independent of non-standard cosmological ingredients and astrophysical systematics. This is analogous to Solar System tests of gravity, and corresponds to testing the equivalence of the two Newtonian-gauge metric potentials. This and related tests are discussed further in the Snowmass-2013 paper on Novel Probes of Gravity and Dark Energy [5].

3.4. Parametrizing growth

Within the canonical picture of General Relativity with smooth, late-time, uncoupled dark energy, the expansion history measured by probes of the recent Universe completely determines the growth history of structure in the recent Universe. However many families of dark energy models lie outside this picture, and it is important to have methods to detect this and characterize the deviations in growth, ideally in a model independent manner. In particular, a desired parametrization of growth should accommodate the following physics of dark energy and gravity:

- *Clustering* of dark energy, which can arise from a low sound speed, $c_s^2 \ll 1$, common in many high energy physics motivated models such as Dirac–Born–Infeld or dilaton theories. Clustering enhances perturbations, and while the direct dark energy perturbations are difficult to detect, the increased contribution to the gravitational potential through Poisson's equation can noticeably affect the matter power spectrum. Since perturbations are only effective when the dark energy equation of state deviates from -1, this class of models is most visible when there is a tracking epoch in the early Universe, where dark energy has an attractor solution that may behave like matter or radiation.
- *Early dark energy*, which is the case when dark energy contributes to the energy budget at CMB recombination ($a \sim 0.001,\ z \sim 1000$) much more than we expect for the cosmological constant case – that is, much more than one part in a billion. Note that early dark energy budget contributions up to 7 orders of magnitude larger (that is, up to $\sim$1% of the total matter plus radiation plus dark energy) are allowed by data. Early dark energy affects growth as well, typically suppressing it mildly but over a very long cosmological epoch.
- *Couplings* of dark energy, which are interactions between dark energy and some other sector. While couplings to Standard Model particles are tightly restricted by particle physics data, the possibility remains of couplings to dark matter, massive neutrinos, or gravity (this can also be viewed as modified gravity, discussed above).

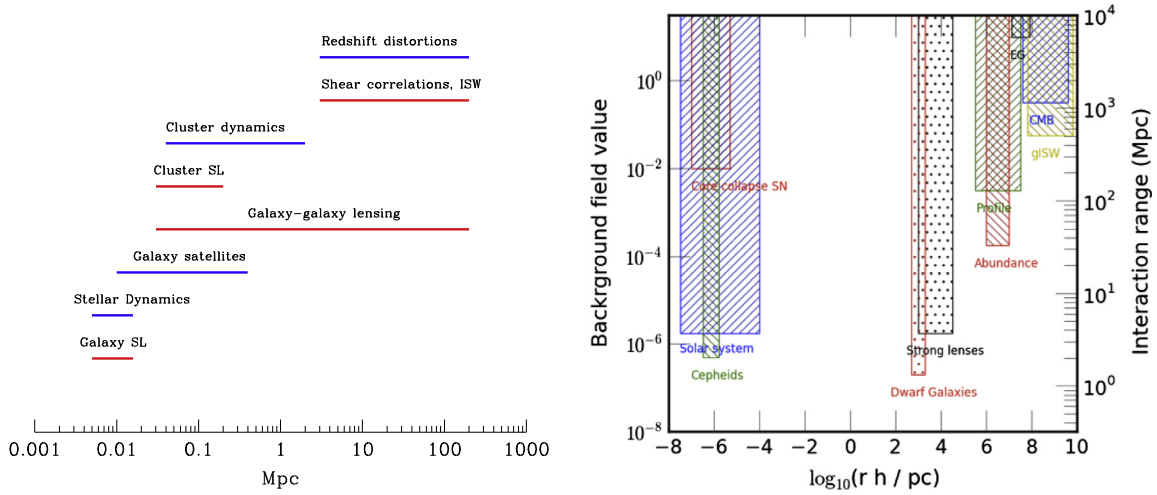

Fig. 3. *Left Panel:* Tests of gravity at different length scales. Red lines shows observations that probe the sum of metric potentials $\Phi + \Psi$ (see Eq. (8)) via e.g. gravitational lensing, while blue lines show dynamical measurements that rely on the motions of stars or galaxies or other non-relativistic tracers and are sensitive to Ψ alone (see Eq. (7)). Adopted from the review by Jain and Khoury [6]. *Right Panel:* Astrophysical [7–9] and cosmological [10–12] limits on chameleon theories. The spatial scale on the x-axis gives the range of length scales probed by particular experiments. The parameter on the *y*-axis is the background field value, or the range of the interaction (*y*-axis label on the right side) for an $f(R)$ model of the accelerating Universe. The rectangular regions give the exclusion zone from a particular experiment. All but the solar system results have been obtained in the last 5 years, illustrating the impressive interplay between theory and experiment in the field. The two rectangles with dots are meant to indicate preliminary results from ongoing work. This figure is adapted from Lombriser et al. [13]. (For interpretation of the references to color in this figure legend, the reader is referred to the web version of this article.)

To connect these families of models most clearly to the observations of growth of large scale structure, while remaining general and reasonably model independent, it is useful to use phenomenological parametrizations that capture the key impact of these dark energy effects on growth. This can be done with a small, remarkably simple set of parameters beyond the equation of state $w(z)$.

The *growth index formalism* provides a general and very simple-to-implement parametrization that can alert that the growth data is not consistently following the expectations from the expansion (distance) data. We define a fitting function for $g(a)$, the linear growth factor divided by a (i.e. with the early matter scaling divided out) in terms of a single free parameter γ

$$g(a) \equiv D(a)/a = \exp\left[\int_0^a (da'/a')[\Omega_M(a')^\gamma - 1]\right], \tag{5}$$

where $\Omega_M(a)$ is the energy density relative to critical at epoch defined by the scale factor a. This formula provides an accurate (0.1% level) approximation for a wide variety of models [14–16]. Within the canonical picture of gravity, $\gamma = 0.55$, almost independently of $w(z)$. This separates out the expansion history as given by $\Omega_M(a)$ from extra growth effects parametrized by deviations of γ from 0.55. If deviations are detected, in the value, scale-, or redshift-dependence of γ, this gives an alert to check noncanonical models, and in particular modifications of gravity (where γ is closely related to the modified Newton's constant $G_{\rm matter}$ introduced below).

Additional parametrizations can shed light on physics behind acceleration. For example, deviations from a purely matter dominated high redshift growth can be parametrized by a growth calibration factor $g_\star$, entering the growth factor as $g = g_{\star} \exp\left[\int_0^a (da'/a')[\Omega_M(a')^{0.55} - 1]\right]$. Note that this form separates out the early time behavior and does not disturb the late time behavior that was parametrized by γ [17]. This test will pick up early dark energy models. Moreover, coupled models can affect the rate of growth – the tug-of-war between gravitational attraction and the stretching apart due to accelerated expansion – at any redshift. This can be treated in the growth factor as [18,19] $g = g_\star(f_\infty) \exp\left[\int_0^a (da'/a')[f_\infty \Omega_M(a')^{0.55} - 1]\right]$. Again, this preserves the late time value of γ, keeping that as a distinct alert. Moreover, since some observations such as redshift space distortions are directly sensitive to the growth rate, one can measure deviations of f_∞ from unity fairly directly. Various other parametrization schemes exist, e.g. [20,21]. Each parametrization has its own strengths and weaknesses: roughly speaking, simpler parametrizations are easier to use and constrain with data, at the expense of having less ability to model the temporal and spatial deviations from GR growth.

Each of these parametrizations serves as an alert that new physics is in play, and moreover they identify the region where the new physics enters – deviation from expansion predictions, at early times, or couplings. Once a deviation is detected, the analysis would then concentrate on more specific models. For clustered dark energy (evident from a scale-dependent $\gamma(k)$) for example, one would then introduce models with a sound speed c_s deviating from the speed of light.

A similar procedure can be applied to the gravitational sector. Modifications of gravity will modify how the nonrelativistic and relativistic gravitational potentials, Φ and Ψ (which govern the motion of matter and of light, respectively), are sourced and evolve. Scalar metric perturbations around a Friedmann–Robertson–Walker background in the conformal Newtonian gauge are given by the following spatial metric

$$ds^2 = -a^2(\tau)\left[(1+2\Psi)d\tau^2 - (1-2\Phi)d\vec{x}^2\right], \tag{6}$$

where τ and x are the conformal time and distance, respectively. Using a model independent parametrization closely tied to the observations, one can modify the Poisson equations relating matter growth $\delta(a)$ to the potentials Φ and Ψ. For example,

$$\nabla^2\Psi = 4\pi G_N a^2 \delta\rho \times G_{\rm matter}, \tag{7}$$

$$\nabla^2(\Phi + \Psi) = 8\pi G_N a^2 \delta\rho \times G_{\rm light}. \tag{8}$$

Any deviations of dimensionless numbers $G_{\rm matter}$ or $G_{\rm light}$ from unity alerts us to possible modifications of General Relativity. The scale- and time-dependence of these parameters can be modeled with independent (z,k) bins [22], eigenmodes [23], or well behaved functional forms [24–27].

4. Cosmological probes sensitive to growth

We now proceed to describe how several of the most promising types of cosmological measurements – clustering of galaxies in spectroscopic surveys, counts of galaxy clusters, and weak gravitational lensing – probe the growth of structure.

4.1. Clustering in spectroscopic surveys

As a natural consequence of large spectroscopic BAO programs such as the Baryon Oscillation Spectroscopic Survey (BOSS) [28], clustering in the density field is sampled at high fidelity in three dimensions over a wide redshift range.

The galaxies and quasars observed in spectroscopic surveys are biased tracers of underlying structure, that is, $\delta_g(z,k) = b(z,k)\delta(z,k)$ where δ_g and δ are the galaxy and dark matter overdensities respectively. The factor b is called the galaxy bias – a time- and scale-dependent number which encodes the basic fact that massive tracers correspond to peaks in the dark matter density field and thus cluster more strongly. The fact that bias multiplies the dark matter overdensity implies a degeneracy between the amplitude $\sigma_R(a)$ of matter fluctuations and parameters describing bias. This degeneracy complicates the extraction of the growth function from the isotropic power spectrum derived from clustering of cosmic sources. However, spectroscopic surveys encode additional information about the velocity field arising from gravitational collapse by separately measuring the power spectrum along and perpendicular to the line of sight. Because the matter distribution directly determines the velocity field, these observations can be used to break the degeneracy between bias and $\sigma_R^2(a)$. Measurements of the velocity field help differentiate between the effect of dark energy and modified gravity as the source of the accelerating Universe through measurements of Redshift-Space Distortions (RSD) [29]. RSD were identified by the recent "Rocky III" report as "among the most powerful ways of addressing whether the acceleration is caused by dark energy or modified gravity," as well as a tool to increase the dark energy Figure of Merit from spectroscopic surveys.

RSD arise because the gravitational pull of matter over-densities causes velocity deviations from the smooth Hubble flow expansion of the Universe. These peculiar velocities are imprinted in galaxy redshift surveys in which recessional velocity is used as the line-of-sight coordinate for galaxy positions, leading to an apparent compression of radial clustering relative to transverse clustering on large spatial scales (a few tens of Mpc). On smaller scales (a few Mpc), one additionally observes the "finger-of-God" elongation [30] due to random velocities of galaxies in a cluster. The resulting anisotropy in the clustering of galaxies is correlated with the speed at which structure grows; deviations from GR causing slower or faster growth give smaller or larger anisotropic distortions in the observed redshift-space clustering. RSD are sensitive to the rate of change of the amplitude of clustering,

$f\sigma_8(a) = d\sigma_8(a)/d\ln a$, where $a = (1+z)^{-1}$ is the dimensionless cosmic expansion factor and $f \equiv f(a)$ has been defined in Eq. (4). Because RSD measurements are sensitive to the product of the growth rate and the amplitude of matter fluctuations, a wide range in redshift coverage is essential to constrain the evolution in clustering amplitude and directly probe GR. On the other hand, if one were to assume a ΛCDM model where GR correctly explains gravitational collapse, the growth rate can be predicted to high precision and RSD results can be used to constrain $\sigma_8(a)$, thereby providing insight into other fundamental physics such as neutrino masses.

Some of the earlier measurements of RSD were obtained by the Two Degree Field Galaxy Redshift Survey [31], the Vimos-VLT Deep Survey [32], the 2SLAQ survey [33], the SDSS-II [34–36], and WiggleZ [37]. More recently, Refs. [38,39] presented the first measurements and cosmological interpretation of RSD in the two-year BOSS galaxy sample [40]. Fig. 4 shows their measurement of the correlation function in terms of the line-of-sight separation and transverse separation. The central "squashing" evident in the left panel is due to structure growth. The right panel of the same figure shows the clustering signal on smaller scales; the "finger-of-God" elongation effect from velocities on small scales is visible for small transverse separations but unimportant on the scales of RSD analyzed here. With these results, BOSS constrains the parameter combination $f\sigma_8(a) = 0.43 \pm 0.07$ at the mean redshift of the sources $z = 0.57$ (or $a = 0.64$), improving to $f\sigma_8(a) = 0.415 \pm 0.034$ if assuming a ΛCDM expansion history.

4.1.1. Prospects for future measurements

The Extended Baryon Oscillation Spectroscopic Survey (eBOSS) is the cosmological survey within SDSS-IV, a six year program that will begin in August 2014. eBOSS will provide the first percent-level distance measurements with BAO in the redshift range $1 < z < 2$, when cosmic expansion transitioned from deceleration to acceleration. The targets for eBOSS spectroscopy will consist of: Luminous Red Galaxies (LRGs: $0.6 < z < 0.8$) at a density of 50 deg^{-2}, Emission Line Galaxies (ELGs: $0.6 < z < 1.0$) at a density of 180 deg^{-2}, "clustering" quasars to directly trace large-scale structure ($1 < z < 2.2$) at a density of 90 deg^{-2}, re-observations of faint BOSS Lyman-α quasars ($2.2 < z < 3.5$) at a density of 8 deg^{-2}, and new Lyman-α quasars ($2.2 < z < 3.5$) at a density of 12 deg^{-2}.

The extended redshift range of the combined eBOSS and BOSS measurements will significantly reduce the degeneracy between $f(a)$ and $\sigma_8(a)$. The wide redshift range of the eBOSS tracers will allow a separation of the evolution of structure growth from the amplitude of clustering and provide new constraints on GR through RSD analyses, or provide tight constraints on σ_8 in the assumption of ΛCDM. The projections on RSD constraints from eBOSS are computed from a Fisher matrix formalism assuming measurements of large-scale modes with wavelengths up to $k_{max} = 0.2$ h Mpc^{-1}. The expected 68% confidence constraints on the growth of structure, parametrized as $f\sigma_8(a)$ and measured from RSD, are $\sigma_{f\sigma_8(a)}/f\sigma_8(a) = 0.029, 0.035$, and 0.036 for the LRG, ELG, and quasar programs respectively.

Prime Focus Spectrograph (PFS) will be a powerful spectroscopic survey of faint emission galaxies because of its large multiplex gain and the 8.2 m aperture of the Subaru telescope [41]. The extended wavelength coverage provided by the red and near-infrared spectrograph arms (650–1260 nm) will permit a survey of about 2×10^6 [O II] emission-line galaxies extending over the redshift range $0.8 < z < 2.4$. As large-scale structure is still in the linear regime at high redshift, such a deep survey will give detailed new information on the cosmological parameters as well as the growth of structure. Multi-color data planned to arrive from the Hyper Suprime Cam (HSC) imager will be used to select target galaxies for spectroscopy. The proposed PFS cosmology survey will consist of 100 nights of observations surveying over 1400 sq. deg., sampling galaxies within a comoving volume of 9 (Gpc/h)^3. This will complement the lower redshift survey being undertaken by the BOSS collaboration. Apart from accurately measuring the dark energy parameters and being sensitive to the presence of early dark energy from the geometrical BAO measurements, PFS will measure the RSD out to redshift $z = 2.4$, and provide the measurement of $f(a)$ to 6% accuracy in each of six bins spanning its redshift range [41]. These PFS measurements of the large scale galaxy distribution can be combined with complementary weak lensing information from the HSC survey in order to improve the growth constraints and reduce uncertainties arising from galaxy bias and nonlinearities that are otherwise major sources of systematic error in spectroscopic surveys.

Dark Energy Spectroscopic Instrument (DESI) will be the largest and most powerful ground-based spectroscopic survey. DESI will provide a comprehensive survey of at least 14,000 deg^2 with an order of magnitude more spectroscopic galaxies and quasars than obtained in BOSS and eBOSS combined. As with eBOSS, the primary targets will be derived from LRG, ELG, and quasars selected from imaging data. The redshift ranges will be refined to probe the

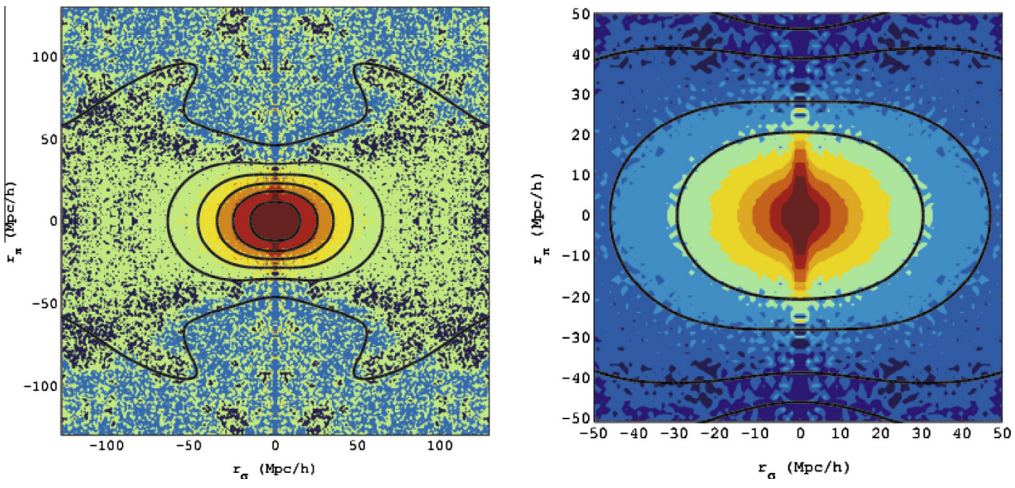

Fig. 4. *Left panel*: Two-dimensional correlation function of BOSS galaxies (color) compared with the best fit model (black lines). Contours of equal ξ are shown at [0.6, 0.2, 0.1, 0.05, 0.02, 0]. *Right panel*: Smaller-scale two-dimensional clustering with model contours at [0.14, 0.05, 0.01, 0]. Figures adopted from Ref. [38]. (For interpretation of the references to color in this figure caption, the reader is referred to the web version of this article.)

$z > 0.6$ epochs at higher resolution than eBOSS: LRG targets will cover $0.6 < z < 1.0$, ELG targets will cover $0.6 < z < 1.5$, and quasar targets will cover $1 < z < 3.5$. In projecting RSD constraints, we assume a 14,000 deg^2 survey with densities 1325 deg^{-2}, 300 deg^{-2} and 176 deg^{-2} for ELG, LRG, and quasars, respectively. Because the number density of galaxies is sufficient to provide RSD constraints in finely binned samples ranging from $0.1 < z < 1.8$, we do not report all of the projections here. The expected 68% confidence constraints from RSD, following the same assumptions as above, are shown in Fig. 2. The precision in each bin ($\Delta z = 0.1$) is better than 2% from $0.4 < z < 1.5$, while the aggregate accuracy from the combination of all three tracers is $\sigma_{f\sigma_8(a)}/f\sigma_8(a) = 0.0035$.

4.1.2. Challenges in RSD constraints

The RSD projections are calculated using the methodology of [42], which assumes that the shape of the power spectrum and the cosmological distance-redshift relationship are known perfectly. While this method produces predictions that are thus independent of additional data sets, marginalization over the power spectrum shape and distance-redshift relationship can potentially degrade the growth constraints. For BOSS, the remaining uncertainty on the shape of the power spectrum is negligible, given a prior from the cosmic microwave background. Imperfect knowledge of the cosmological distance-redshift relationship induces additional anisotropy in the observed galaxy correlations via the Alcock–Paczynski effect [43–45] that is partially degenerate with the RSD-induced anisotropy. The Alcock–Paczynski effect depends on the product $D_A(a)H(a)$, where D_A is the angular diameter distance and H is the Hubble parameter. However, allowing for an arbitrary value of $D_A(a)H(a)$ degraded $f\sigma_8$ constraints by a factor of two in BOSS. Marginalizing over additional parameters in nonlinear galaxy biasing and small-scale Finger-of-God velocities may further slightly degrade the errors (by 10% for BOSS DR9 analysis).

RSD have, until recently, been modeled using a simplistic separation of density and velocity correlations. This separation is known to be inaccurate especially at smaller scales, where non-linear growth ($\delta > 1$) couples density and velocity modes at different scales. It is going to be necessary to simulate and understand these correlations to sufficient precision to avoid systematic errors, from imprecise modeling, that degrade the reconstruction of the growth of structure from RSD observations [46].

Finally, the projections assume that spectroscopic large-scale clustering measurements will be limited by statistical errors. This requires stringent control of systematic errors that can modulate the data on varying scales, such as the impact of stellar contamination and dust extinction on target selection efficiency, variations in seeing that alter target selection and redshift success, and so on. These systematics have already been extensively studied within BOSS [47,48], and the greater volume and greater statistical power at large scales from eBOSS and DESI will place new demands on homogeneity of the target samples. Lessons from BOSS are being applied to target selection in eBOSS. Similarly, better understanding of these systematics learned during eBOSS will provide important information for preparation of target selection in DESI.

Given the potential for providing dark energy measurements, constraints on fundamental neutrino and inflation physics, and cluster redshifts, velocity dispersions, and calibration of photometric redshifts for large imaging programs, it is clear that wide-field optical spectroscopy will play a central role in cosmology well after the completion of DESI. At this time, it is impossible to estimate the exact details of such a program, but detector technology, full integration of robotic fiber positioners into large surveys, and likely availability of large telescopes paint a clear path for ground-based spectroscopic surveys beyond DESI. One can imagine an order of magnitude increase in the number of fibers per field of view, sensitivity at least one magnitude fainter than that of DESI, and wavelength coverage extending in the near infrared. The *WFIRST* and *Euclid* missions both incorporate near-IR, slitless spectroscopic surveys that are expected to detect tens of millions of emission line galaxy redshifts in the range $0.5 < z < 2$.

Precise modeling of target source populations, their respective number densities and redshifts is beyond the scope of this document. In addition, the power of these surveys will likely only be fully realized when the theoretical models of structure formation adequately describe the velocity field measured in non-linear and mildly non-linear regimes. Theoretical developments in the growth of structure are discussed in more detail in Section 5.

4.1.3. Other uses of clustering to probe growth

Along with the geometric information from baryon acoustic oscillations, the growth information from the RSD is thought to provide the most promising and reliable method that uses clustering of galaxies to measure dark energy properties. However, growth can be probed using several other methods that use either photometric or spectroscopic galaxy surveys, and here we cover them briefly.

The broadband power spectrum of galaxies or other tracers of the large-scale structure, $P(k, a)$, can be measured to excellent accuracy over several decades in k. On linear scales, the power spectrum is proportional to $D(a)^2$, and hence it directly probes the growth of structure. Unfortunately, the power spectrum is also proportional to the bias of the tracer objects, and this bias is typically *also* time and scale-dependent, albeit in a way that often has to be extracted from the data itself. It is therefore challenging to obtain accurate constraints on the growth of structure from the broadband $P(k, a)$ measurements alone. On the other hand, combining the broadband power measurements that are sensitive to bias with weak lensing measurements that are not can be used to break this bias-growth degeneracy. This is one of the manifestations of the powerful synergy between the spectroscopic and photometric surveys.

The cross-correlation between the galaxy density field and the hot and cold spots in the CMB anisotropy maps is directly sensitive to the Integrated Sachs-Wolfe (ISW) effect, and thus probes the decay of the gravitational potential due to the presence of dark energy at late times. These measurements produced independent evidence for dark energy and have achieved increased accuracy over the years (e.g. [49–51]). However the largest signal available from the cross-correlation corresponds to about 10-σ detection of the effects of dark energy via the ISW effect [52], making it a probe with relatively modest prospects.

Cosmic magnification, discussed in more detail in the Snowmass-2013 paper on Cross-Correlations and Joint Analyses [53], induces additional spatial correlations between the density, luminosity, and size of objects due to the bending of light by structures located between those objects and the observer. The full potential of magnification measurements to probe dark energy is only beginning to be explored.

4.2. Cluster abundances

4.2.1. Clusters abundances as a probe of fundamental physics

Galaxy clusters are the most massive gravitationally bound structures in the Universe. As with other dynamical probes, their primary importance in the context of dark energy is their complementarity to geometric probes, i.e. their ability to distinguish between modified gravity and dark energy models with degenerate expansion histories. For a complete review, we refer the reader to Refs. [54,55].

The basic physics behind cluster abundances as a cosmological probe are conceptually simple. Clusters form the gravitational collapse of density fluctuations. Prior to collapse, the growth of these fluctuations is linear, so that the matter density contrast $\delta = \delta\rho/\rho$

at *any* spatial scale evolves with the same growth factor $D(a), \delta(a) \propto D(a)$, where the linear growth factor $D(a)$ can be evaluated exactly for a given cosmological model following Eq. (1).

At some critical threshold δ_c, the perturbation undergoes gravitational collapse. Consequently, the probability of forming a halo – a collapsed object – is equivalent to the probability that $\delta \geqslant \delta_c$. Assuming Gaussian random initial conditions, one finds then that the number of collapsed objects N per unit mass dM and comoving volume element dV is

$$\frac{dN}{dMdV} = F(\sigma)\frac{\rho_M}{M}\frac{d\ln\sigma^{-1}}{dM}, \tag{9}$$

where ρ_M is the matter density in the Universe, σ^2 is the variance of the density perturbations evaluated at some mass scale M (or, equivalently, spatial scale R where $M = (4\pi/3)R^3\rho_M$). Here $F(\sigma)$ corresponds to the fraction of mass in collapse object; in the Press–Schechter argument [56],

$$F(\sigma) = \frac{1}{\sqrt{2\pi\sigma^2}}\exp\left(-\frac{1}{2}\frac{\delta_c^2}{\sigma^2}\right), \tag{10}$$

while cosmological N-body simulations have been used to calibrate $F(\sigma)$ to higher precision beyond the simple Press–Schechter formula.

It is precisely this dependence of the number of galaxy clusters on the variance of the *linear* density field that allows us to utilize galaxy clusters to constrain the growth of structure. In particular, the late-time variance of the linear density field $\sigma^2 \equiv \sigma^2(a)$ is related to the variance at some initial scale factor a_0, σ_0^2, via the linear growth function, $\sigma^2 = [D^2(a)/D^2(a_0)]\sigma_0^2$, which makes the abundance of galaxy clusters explicitly dependent on the growth history of the Universe.

A cluster abundance experiment is conceptually very simple: one first identifies galaxy clusters – e.g. as cluster of galaxies in the optical, as extended sources in the X-rays, or as Sunyaev–Zel'dovich (SZ) sources (cold spots in the CMB) at millimeter wavelengths – and then one needs to determine the corresponding cluster masses. As noted below, future surveys will almost certainly rely on weak lensing mass calibration to estimate cluster masses. Fig. 5, taken from Ref. [55], shows forecasted constraints on the amplitude of matter fluctuation $\sigma_{11,\mathrm{abs}}$ for two fiducial 10^4 deg^2 surveys, assuming 10 gals/arcmin^2 and a shape noise appropriate for ground-based observations ($\sigma_e = 0.4$), and for a similar survey with 30 gals/arcmin^2 and a shape noise appropriate for space-based observations ($\sigma_e = 0.3$). These forecasts are compared to the predictions for Stage III (blue curve) and Stage IV (red curve) *Planck* + weak lensing + supernova + BAO experiments. We see that galaxy clusters are statistically competitive with and often better than other probes, highlighting their complementarity as a discriminant between dark energy and modified gravity models.

Galaxy clusters can probe dark energy in other ways as well, most notably by comparing cluster mass estimates from weak lensing and dynamical methods such as galaxy velocity dispersions; see Section 3. In addition, because the growth of structure is also impacted by non-zero neutrino mass, galaxy cluster abundances can provide competitive constraints on the sum of neutrino masses, further enhancing their value as a tool for fundamental physics (e.g. [57–60]).

4.2.2. Systematics: current limitations and future prospects

Galaxy clusters can be identified with optical, mm, or X-ray data. Regardless of how the clusters are identified, the cosmological utility of cluster samples is always limited by our ability to estimate the corresponding cluster masses. Roughly speaking, CMB + geometric probes predict the amplitude of matter fluctuations as a function of redshift with $\approx 3\%$ (0.9%) precision for Stage III (IV) dark energy experiments. To achieve comparable levels of precision using galaxy clusters, we must be able to measure cluster masses with $\approx 5\%$ (2%) precision [55].

While this level of precision is significantly better than what has been achieved to date, there are good reasons to believe that it can be achieved in the near future. Specifically, most cosmological work to date has relied on hydrostatic X-ray mass estimates, which are subject both to departures from hydrostatic equilibrium (e.g. [61–64]) and X-ray calibration uncertainties [65,66]. Future work, however, will rely on weak lensing mass calibration, which entirely bypasses the aforementioned systematics at the expense of new, better controlled systematics.

The two primary sources of systematic errors for weak lensing mass calibration are shear biases, i.e. systematic uncertainties in our estimates of the gravitational shear, and systematic errors in the redshift distribution of the photometric lensing sources. Where the systematic floor of these type of measurements ultimately remains to be seen, with the most recent analyses suggesting that $\approx 7\%$ mass calibration has been achieved. We caution, however, that $\approx 20\%$ systematic offsets between different groups remain [67].

The reduction of shear and photometric redshift systematics is the thrust of ongoing investigations. Shear estimation methods are being tested and improved upon via extensive simulation tests [68–71], and the possibility of self-calibrating systematics from joint shear and magnification analyses of the weak lensing signal has been noted [72–75]. In addition, the use of spectroscopic sources for weak lensing mass calibration [76] entirely bypasses

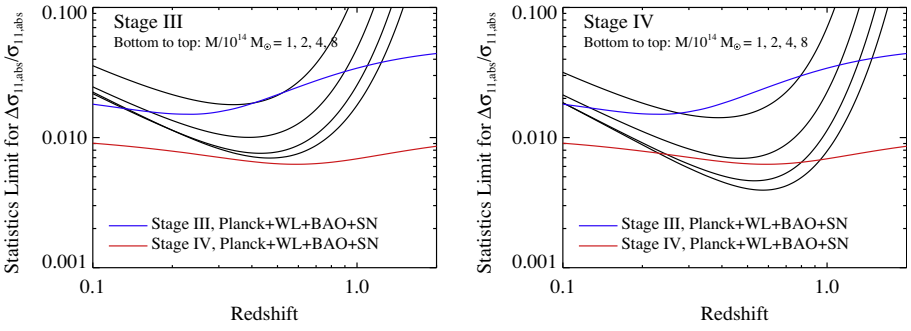

Fig. 5. Statistical error on $\sigma_{11,\mathrm{abs}}(z)$ – or equivalently the growth function $D(a)$ – derived using galaxy clusters in redshift bins of width $z \pm 0.05$ for two fiducial 10^4 deg^2 surveys: *Left panel*: a Stage III survey with shape noise appropriate for ground-based imaging (source surface density 10 gals/arcmin^2, shape noise $\sigma_e = 0.4$); *Right panel*: a Stage IV survey with shape noise appropriate for space-based imaging (30 gals/arcmin^2, $\sigma_e = 0.3$). Each solid black line corresponds to a different mass threshold, as labeled. The blue and red curves are the corresponding constraints from Stage III (blue) and Stage IV (red) weak lensing + supernova + BAO + *Planck* experiments. Figure taken from Ref. [55]. (For interpretation of the references to color in this figure legend, the reader is referred to the web version of this article.)

both sources of systematic errors. Similarly, photometric redshift errors have been the focus of several recent theoretical works aimed specifically at understanding how to minimize this source of systematic uncertainty (e.g. [77–79]). Alternatively, as discussed in the Snowmass-2013 white paper on the Spectroscopic Needs for Imaging Dark Energy Experiments [80], cross-calibration methods may provide an effective alternative to photometric redshift biases [81,82]. In short, *there are very good reasons to believe that the systematic floor in current weak lensing measurements will be significantly reduced in the future.*

Systematic errors in shear measurements tend to be less critical for cluster abundance work than for cosmic shear work, partly because of the existence of a preferred orientation *a priori* (we are interested in tangential shear), partly because of circular averaging of the shear (which removes systematics that fluctuate on scales larger than a galaxy cluster), and partly because the weak lensing signal of clusters is large relative to the typical shear signal. The impact of photometric redshifts on both data sets, however, is fairly comparable. Overall, one can fairly generically state that experiments that control shear systematics at a level that enables cosmic shear experiments also automatically enable cluster weak lensing mass calibration.

There are, however, additional (currently sub-dominant) sources of systematics that can impact galaxy clusters. Key amongst these is the calibration not only of the mean relation between cluster observables (optical, X-ray, or mm signals) and cluster mass, but also the scatter (shape and amplitude) about the mean. Estimates (e.g. [83]) suggest that $\approx 5\%$ calibration of this scatter – which is achievable today – is sufficient for near future experiments (e.g. DES, HSC, PanSTARRS), but this source of error is likely to become significant for Stage IV surveys such as Large Synoptic Survey Telescope (LSST), *Euclid*, and *WFIRST*, and certainly for any putative Stage V experiment, simply because these surveys will have very small statistical errors. Such calibrations should be achievable with high resolution X-ray imaging using high quality mass proxies like M_{gas} or Y_X. Note that these proxies will themselves be calibrated via weak lensing, so the hydrostatic bias noted above for X-ray mass calibration is irrelevant in this context.

In addition, cluster centering remains an important systematic in optical and/or low resolution experiments (e.g. *Planck*). Specifically, weak lensing mass calibration requires we measure the tangential shear of background galaxies centered on galaxy clusters, but selecting the center of a galaxy cluster is not always trivial. This systematic can either be self-calibrated [84], or it may be calibrated with high resolution X-ray/mm follow-up of small sub-samples optical galaxy clusters. Note that optical cluster detection is still highly desirable, as optical observations benefit from a lower mass detection threshold than X-ray/mm over a large redshift range, which in turn result in improved statistical constraints. Thus, the combination of optical with X-ray and mm data is clearly superior than either data set alone.

The synergistic nature of multi-wavelength cluster cosmology will necessarily play a key role in future cluster abundance experiments. Clusters are fortunate in that they can be studied across the electromagnetic spectrum, and consistency between all measurements provide critical self-consistency constraints that can ferret out hitherto undetected systematics [85]. Moreover, multi-wavelength cluster abundance studies can further improve cosmological constraints relative to what can be achieved with single wavelength measurements [83,86]. Consequently, a balanced multi-wavelength approach will be critical to the success of cluster cosmology over the next 10–20 years.

One final key prospect with galaxy clusters remains, that of self-calibration. That is, the cluster-clustering signal is itself an observable that one can use to calibrate cluster masses, and which is insensitive to all of the above systematic effects. In general, self-calibration does result in some degradation of cosmological information relative to systematics-free weak lensing measurements, but such loss decreases with a decreasing mass threshold. Provided one can reach low cluster masses, e.g. in the optical, self-calibration is an attractive option. Indeed, multiple studies have found that self-calibration of galaxy clusters are capable of placing cosmological constraints that are comparable to those from cosmic shear analysis in the absence of systematics [87,84].

4.2.3. Cluster wish lists

The minimum necessary data for Stage IV cluster experiments should be immediately available from LSST, *Euclid*, and *WFIRST* in the optical/IR, eRosita in the X-rays, and *Planck*, and the new generation South Pole Telescope (SPT) and Atacama Cosmology Telescope (ACT) experiments. We emphasize that scatter calibration – regardless of the origin of the clusters – will require high resolution X-ray imaging, so large follow-up programs with existing instruments (Chandra, XMM) is a must. The commissioning of new, more sensitive high resolution X-ray satellites is particularly important for studying the lower mass, higher redshift systematics that should dominate the next generation of cluster cosmology experiments. In the mm, next generation surveys such as SPT3G and beyond will allow for better mass calibration and systematics control of optical surveys at low cluster masses, as well as SZ detection of higher redshift systems. Continuing improvement in mm detector technology will remain a fruitful enterprise from the point of view of cluster cosmology.

In addition, spectroscopic follow-up of 2 + bright galaxies in galaxy clusters is highly desirable. As an example, in its Spectroscopic Identification of eROSITA Sources (SPIDERS) program, eBOSS will acquire several redshifts per cluster by observing objects associated with eROSITA X-ray clusters but not included in the BOSS and eBOSS galaxy clustering samples. Such a follow-up program will lead to improved cluster centering, better photometric redshift performance and calibration, and it would enable testing of modified gravity models by comparing dynamical to weak lensing masses via correlation methods. Note that this program could easily be included as part of a spectroscopic program targeting LRGs, as these type of galaxies dominate the cluster population, an obvious "value added" to spectroscopic BAO surveys, provided the spectroscopic and cluster surveys overlap. Similarly, spectroscopic follow-up of background galaxies at high redshift for BAO studies (e.g. emission-line galaxies) enables spectroscopic weak lensing measurements, which are insensitive to both shear and photometric redshift systematics. These spectroscopic samples also allow for photometric redshift calibration via cross-correlation methods, which will reduce systematic error uncertainties in the redshift distributions of photometric source galaxies. In short, from a cluster perspective, overlap of cluster surveys with spectroscopic BAO experiments clearly provides a value added to clusters that is otherwise unavailable. A quantification of these gains, however, is difficult, as the value of such measurements will likely depend on the systematic floor of shear-based weak lensing mass measurements with photometric sources.

4.3. Weak gravitational lensing

4.3.1. Background

The gravitational bending of light by structures in the Universe distorts or shears the images of distant galaxies. This distortion allows the distribution of dark matter and its evolution with time to be measured, thereby probing the influence of dark energy on the growth of structure.

Within the past decade, *weak gravitational lensing* – slight distortions of galaxy images due to the bending of the light from distant galaxies by the intervening large-scale structure – has become

one of the principal probes of dark matter and dark energy. The weak lensing regime corresponds to the intervening surface density of matter being much smaller than some critical value. While weak lensing around individual massive halos was measured in the 1990s [88,89], weak lensing by large-scale structure was eagerly expected, its signal predicted by theorists around the same time [90–92]. In this latter regime, the observed galaxies are slightly distorted (roughly at the 1% level) and one needs a large sample of foreground galaxies in order to separate the lensing effect from the noise represented by random orientations of galaxies.

A watershed moment came in the year 2000 when four research groups nearly simultaneously announced the first detection of weak lensing by large-scale structure [93–96]. Since that time, weak lensing has grown into an increasingly accurate and powerful probe of dark matter and dark energy [97–107]. Below we first briefly summarize how weak lensing probes dark energy and in particular the growth of structure; more detailed reviews of the topic are available in [108–110].

4.3.2. Shear measurements and cosmological constraints

The statistical signal due to gravitational lensing by LSS is termed cosmic shear. The cosmic shear field at a point in the sky is estimated by locally averaging the shapes of large numbers of distant galaxies. The primary statistical measure of the cosmic shear is the shear angular power spectrum, which is measured as a function of the source-galaxy redshift z_s. Additional information is obtained by measuring the correlations between shears at different redshifts, which is referred to as 'shear tomography', or between shears and foreground galaxies – the "galaxy–galaxy lensing".

The principal power of weak lensing comes from the fact that it responds to all matter, both dark and baryonic, and not just to visible (or, more generally, baryonic-only) matter like most other probes of the large-scale structure. Therefore, modeling of the visible-to-dark matter bias, a thorny and complicated subject, is altogether avoided when using weak lensing. Simulations of dark matter clustering are becoming increasingly accurate, and simulation-based predictions that include baryons (which steepen and therefore affect the dark matter halo density profiles [111–113]) should be able to reach the accuracy required to model the weak lensing signal so that modeling errors do not appreciably contribute to the total error budget. Because of our ability to model its signal accurately, weak lensing has great intrinsic power to probe dark matter and dark energy in the Universe.

The other principal reason why weak lensing is powerful comes from the fact that *galaxy shear is sensitive to both geometry and the growth of structure*. Gravitational lensing depends on the geometry (e.g. location of the lens relative to the source and the observer and the mutual distances involved), while the growth determines how much structure is available at a given distance to serve as cosmic lenses for light coming from even more distant galaxies. In particular, in the so-called Limber approximation and assuming small shear, one can write the two-point correlation function of shear in harmonic space as [114]

$$P^{\kappa}_{ij}(\ell) = \int_0^{\infty} dz \underbrace{\frac{W_i(z)\,W_j(z)}{r(z)^2\,H(z)}}_{\text{geometry}} \underbrace{P\left(\frac{\ell}{r(z)}, z\right)}_{\text{growth}}, \tag{11}$$

where each integer multipole ℓ corresponds to angular scale of about $180^\circ/\ell$. Here $r(z)$ is the comoving angular diameter distance, $H(z)$ is the Hubble parameter, the weights W_i are given by $W_i(\chi(z)) = \frac{3}{2}\,\Omega_M\,H_0^2\,g_i(\chi)\,(1+z)$ where $g_i(\chi) = r(\chi)\int_{\chi}^{\infty} d\chi_s n_i(\chi_s) r(\chi_s - \chi)/r(\chi_s)$, and n_i is the comoving density of galaxies if the coordinate distance to source galaxies $\chi_s \equiv \chi(z_s)$ falls in the distance range bounded by the ith redshift bin and zero otherwise. Therefore, weak lensing probes the growth directly via the redshift-dependence[2] of the power spectrum $P(k,z)$ in Eq. (11).

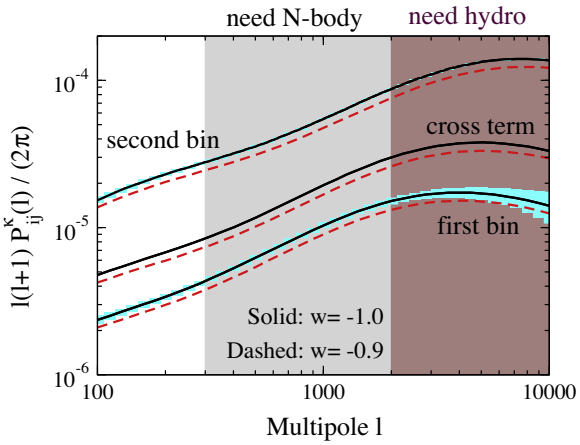

Fig. 6. Cosmic shear angular power spectrum and statistical errors expected for a future survey such as the LSST. We show two dark energy models with equations of state $w = -1$ and -0.9; modified gravity theories will also be probed but are not shown. For illustration, results are shown for source galaxies in two broad redshift bins, $z_s = 0$–1 (first bin) and $z_s = 1$–3 (second bin); with expected good quality of photometric redshifts a much finer slicing of source galaxies in redshift may be employed. The cross-power spectrum between the two bins (cross term) is shown without the statistical errors. Shaded regions show scales on which pure gravity and hydrodynamic simulations, respectively, are necessary to model the theory; this is further discussed in Section 5. Adaptation of a plot from Ref. [115].

The statistical uncertainty in measuring the shear power spectrum is

$$\Delta P^{\kappa}_{ij}(\ell) = \sqrt{\frac{2}{(2\ell+1) f_{\rm sky}}}\left[P^{\kappa}_{ij}(\ell) + \delta_{ij}\frac{\langle\gamma^2_{\rm int}\rangle}{\bar{n}_i}\right], \tag{12}$$

where $f_{\rm sky}$ is the fraction of sky area covered by the survey and δ_{ij} is the Kronecker delta function. The first term in brackets, which dominates on large scales, comes from cosmic variance of the mass distribution, and the second, shot-noise term results both from the variance in galaxy ellipticities ("shape noise") and from shape-measurement errors due to noise in the images. Therefore, to achieve the best weak lensing measurements, we aim to maximize sky coverage (i.e. maximize $f_{\rm sky}$); to minimize the shape noise $\langle\gamma^2_{\rm int}\rangle$; and to be able to theoretically model and experimentally measure shear to as small a scale (high ℓ) as possible.

Fig. 6 shows the cosmic shear angular power spectrum and statistical errors expected for a future survey such as LSST. We show two dark energy models with equations of state $w = -1$ and -0.9; modified gravity theories will also be probed but are not shown. For each cosmology, there are two curves for the auto-correlations of the shears in two different redshift bins, and one curve for the cross-correlation of the shears between the two redshift bins. Depending on the quality of photometric redshifts, a much finer slicing of source galaxies in redshift may be employed. The difference between the two equations of state is much larger than the statistical errors expected for LSST (or other planned Stage IV surveys). The shaded regions in Fig. 6 show regimes in which dark-matter-only simulations, and hydrodynamical simulations with baryons, respectively will be required in order to calibrate the theoretical angular power spectrum.

In addition to the angular power spectrum, other statistics have been developed, which have only a somewhat lower statistical

[2] The separation of the growth and geometry dependencies outlined in Eq. (11) is slightly inaccurate, since the number density of source galaxies, $n_i(\chi_s)$, which is in the weights $W_i(z)$, technically falls in the growth category.

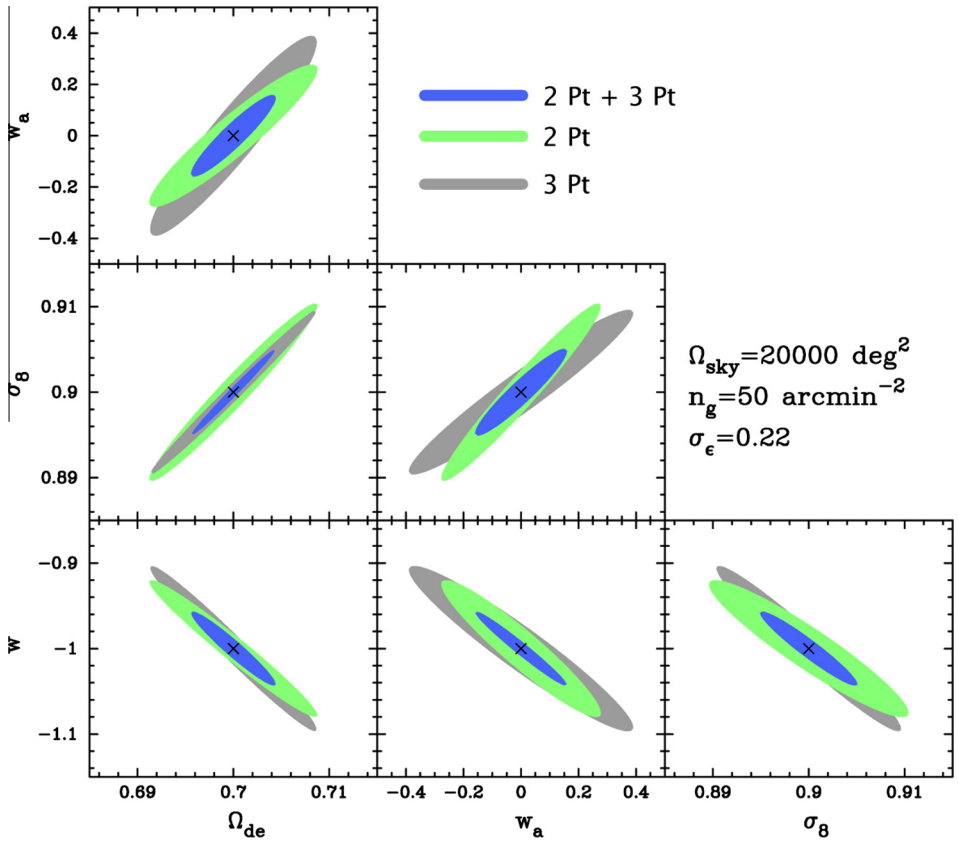

Fig. 7. Forecasted constraints on cosmological parameters, assuming LSST's weak lensing data. We show the 68% confidence limit contours for the two-point and three-point correlation functions separately (green and gray, respectively), as well as the combined constraints using both measurements (blue). These assume priors on the spectral index n_s, physical baryon density $\Omega_b h^2$ and scaled Hubble constant $h \equiv H_0/(100\ \mathrm{km/s/Mpc})$ from the *Planck* mission. Adopted from Ref. [116].

power, but which cut through parameters space differently, so combining them with the power spectrum can produce significantly better overall constraints on dark energy parameters. Fig. 7 shows the improved dark energy constraints that are possible by combining the three-point shear correlation function (related to the dark matter bispectrum) with the two-point correlation function (related to the power spectrum). Because the contours are somewhat orthogonal to each other in parameter space, the resulting combined constraints are much better than either one individually. The constraints shown in Fig. 7 take advantage of the ability to measure photometric redshifts for the lensed galaxies. Not only does this improve the calibration of the source population compared to what is possible with current surveys, but it also allows us to use multiple redshift slices (five in this example) for the auto- and cross-correlation measurements.

The three-point function is merely the simplest statistic that probes the non-Gaussianity of the underlying dark matter distribution. Others include lensing peaks which provide information similar to that provided by galaxy clusters but are sensitive to all mass, (e.g. [117]), moments of the convergence distribution, and Minkowski functionals (e.g. [118]). These statistics show excellent potential to improve the weak lensing power spectrum constraints on dark energy.

Finally, weak gravitational lensing is particularly useful probe of modified gravity. Gravitational lensing observations in general are sensitive to the sum of the two gravitational potentials $\Phi + \Psi$ (see Eq. (8)), while particle dynamics probes Ψ alone (e.g. [119–121]). Since modifications to gravity typically affect the two potentials differently, combination of weak lensing with other cosmological probes can in principle be used to differentiate modified gravity from dark energy.

4.3.3. Systematic errors and efforts to control them

While potentially extremely powerful, the underlying shear measurements are subject to a variety of systematic errors. There are numerous potential sources of spurious shear, such as the atmospheric PSF, telescope aberrations and distortions, charge distribution effects in the CCDs, noise rectification biases in the shear measurements themselves (since the underlying measurement is intrinsically nonlinear), to name only the most difficult problems. Obtaining reliable shear estimates has been an ongoing process within the weak lensing community. A series of challenges [68,69,122,70] have been testing our ability to measure shear to the required accuracy. So far, the state of the art has kept pace with the accuracy required for current surveys. However, no one has yet demonstrated a pipeline that can reach that accuracy required for Stage IV surveys. A new challenge, dubbed GREAT3[3] [123] tests pipelines at the accuracy required for these upcoming surveys, and also adds new elements of realism that had been absent in previous challenges.

The interpretation of weak lensing shear measurements is also complicated by the photometric redshift biases [124,77], calibration of the predictions in the non-linear regime from *N*-body simulations [125–127], and non-Gaussian errors on small angular scales [128–130]. Similar to the effort to improve shape measurements, there has also been a large effort to handle these effects to the accuracy that will be required for Stage IV surveys. The requirements are stringent; for example, future surveys need to calibrate the mean shear in each of the ∼10 redshift bins to about 0.1% *relative* accuracy in order that dark energy constraints not be signifi-

[3] http://great3challenge.info/

cantly degraded [131]. However, what really helps weak lensing is the possibility of "self-calibrating" the systematic errors – determining a reasonable set of the systematic error nuisance parameters from the survey concurrently with the cosmological parameters without appreciable degradation in accuracy on the latter. With self-calibration, the survey itself is used to partially calibrate the systematic effects.

Intrinsic alignments of galaxy shapes (e.g. [132]) are a systematic unique to weak lensing, since they lead to possible misinterpretations of galaxy alignments caused by the local tidal field as the cosmic large-scale-structure signal. Many methods that are currently considered promising for tackling it involve marginalizing over parametrized models for this effect [133,134] which, in turn, degrades how well dark energy and modified gravity parameters can be constrained [135,136]. Thus, accurate removal of intrinsic alignments with minimal loss of cosmological information requires fairly tight priors on the scaling of intrinsic alignments with galaxy separation, type, redshift, luminosity, and potentially other parameters. Existing observational constraints (e.g. [137,138]) are limited by the requirement that the galaxy sample have both (a) shear estimates and (b) excellent redshift information (either spectroscopic, spectro-photometric, or very high-quality photo-z) for a reasonably high-density galaxy sample over a contiguous area large enough to find galaxy pairs with separations of $\sim 100h^{-1}$ Mpc. Since several upcoming surveys will provide shape measurements, additional overlapping datasets with redshifts will be very useful in providing constraints on intrinsic alignment models that, in turn, will be used to remove intrinsic alignments from weak lensing measurements by Stage IV surveys. For example, a significant step forward from our current knowledge would come from a survey with DEEP2-like parameters (~ 3 galaxies/arcmin^2 for a fairly-selected sample at $z > 0.7$) but with ten times the area. Since such a survey would be extremely expensive to carry out spectroscopically, spectro-photometric or many-band photometric surveys might be the best option for collecting such a dataset. Note that the requirements are similar to those for spectroscopic samples for photo-z calibration, because we need to span the range of different galaxy types; we do however need a fairly large, contiguous field.

4.4. Weak lensing of the cosmic microwave background

Just as weak gravitational lensing by foreground structure distorts the shape of background galaxies, it also distorts the fluctuations in the cosmic microwave background. In CMB temperature maps, this has the effect of slightly deflecting trajectories of the CMB photons, which in turn distorts the shapes and sizes of the cold and hot spots. In the CMB power spectrum, lensing smoothes the peaks and also induces non-gaussian mode coupling that can be measured via the four-point correlation function. One can readily construct estimators that can be applied to CMB temperature maps to reconstruct the map of the deflection field, which in turn determines the matter distribution and the matter power spectrum integrated over the observed line-of-sight. For a review, see [139].

The CMB lensing power spectrum was measured via the four-point function signal by Atacama Cosmology Telescope (ACT; [140,141]), South Pole Telescope (SPT; [142]), and most recently by Planck [143]. The Planck lensing measurement has a lensing detection significance of 25σ and a 5% constraint on the matter power spectrum. This translates to a 2.5% constraint on σ_8 in this higher redshift range. Future CMB temperature measurements by ACTpol and SPTpol, and their upgrades, will improve these constraints by a factor of two [144].

The angular power spectrum of the *deflection* field obeys equation very similar to Eq. (11), where contributions along the line of sight are a product of a geometrical term and the matter distribution, the latter of which encodes the growth of cosmic structure. The CMB lensing signal is most sensitive to matter in the redshift range $z \sim 2$–4, which is where its window functions, corresponding to $W(z)$ in Eq. (11), peaks. Thus CMB lensing provides an important anchor at high redshifts for growth measurements and tightens dark energy and neutrino mass constraints from lower-redshift growth probes.

For example, in the Doran–Robbers early dark energy model [145], the early dark energy density Ω_e (defined as dark energy density relative to critical at $z \gg 10$) can be mimicked by standard dark energy with a time varying equation of state at late times; the two contributions are indistinguishable by late-time experiments. CMB lensing measurements can break this degeneracy: the combined Planck and ground-based Stage III CMB lensing experiment's data constrain Ω_e to about one quarter of a percent ($\sigma(\Omega_e) = 0.0025$), while simultaneously constraining the sum of neutrino masses to 90 meV (rather than 165 meV from Planck alone in this model) [146]. Note that since both early dark energy and neutrino mass suppress early growth, constraints on neutrino mass tend to be tighter in non-early dark energy models; thus early dark energy models give more conservative bounds.

In addition to generating the lensing signal in CMB temperature maps, lensing also distorts the polarization of the microwave background, turning E-mode polarization into B-mode polarization. This B-mode lensing signal was recently detected by SPTpol [147]. While achieving a lensing detection in polarization maps requires better instrument sensitivity than is needed for temperature maps, the signal is cleaner since there are fewer polarized foregrounds. Sub-percent level constraints on σ_8 from the B-mode lensing signal should be within reach of Stage III ground-based CMB experiments.

Finally, weak lensing of the CMB, when combined with the weak lensing of galaxies by large-scale structure, can be used to partly cancel out pernicious effects of systematic errors in galaxy shear measurements that enter in a multiplicative way [148,149]. This is just one of the useful applications of cross-correlations in cosmology that are further discussed in the Snowmass-2013 paper on Cross-correlations and joint analyses [53].

5. Simulations

5.1. Cosmological simulations of growth of structure

Simulating the dynamical evolution of a representative volume of the observable Universe, using either particles or grids to model relevant fields, is an essential method for understanding the nonlinear growth of structure (see [150] for a recent review). Cosmological simulations enable the generation of synthetic sky catalogs of galaxies or galaxy clusters with different levels of observational complexity. Such synthetic data is now regularly used to interpret survey results, especially to better understand issues related to sample/cosmic variance, projection effects, error covariance, other sources of statistical and systematic uncertainty. In this subsection, we discuss the two main modes of dynamical simulations – N-body with only gravity and hydrodynamical with baryonic physics – and comment on their utility to survey programs.

5.1.1. Gravity-only N-body simulations

N-body simulations evolve the gravitational dynamics of clustered matter, under an implicit assumption that baryons exactly trace the dark matter on the resolved scales of the simulations. This simplifying assumption has the advantage that the calculation is fast and scales efficiently on parallel platforms; to date, simulations with nearly a trillion particles in a volume of several cubic

giga-parsec have been conducted, e.g. DEUS FUR [151], Horizon Run 3 [152], and Millennium-XXL [153] and the trillion-particle milestone was reached in late 2012 [154,155].

N-body simulations are essential for modeling the structure growth at trans-linear and non-linear scales where linear perturbation theory breaks down and higher-order perturbation theory is difficult to perform. In fact, a comparison between *N*-body simulations and higher-order perturbation theory can be used to cross-check the validity of both methods [156]. One of the most important predictions of *N*-body simulations is how the matter power spectrum depends on cosmological parameters [157]; as stated in Section 4.3, an accurate prediction of the matter power spectrum is essential for galaxy clustering and weak lensing shear correlations. In addition, the halo mass function, which was described in Section 4.2, relies on *N*-body simulations for precision calibration [158–163]. It has been shown that for Stage III dark energy experiments, percent-level accuracy in mass function is required to avoid severe degradation of dark energy constraints [164,165]; achieving this level of accuracy will require improved simulations of baryon evolution.

Beyond the standard ΛCDM model, *N*-body simulations of non-standard extensions include explorations of quintessence models [166,167], modified gravity [168–172], coupled dark energy and dark matter [173,174], and self-interacting dark matter [175]. These simulations provide us with insights of how these different models affect the growth of structure, which can be imprinted in the halo mass function, halo bias, and the density profile of halos. A challenge in this area, at least on small scales, is that effects from subtle modifications to the expansion history and linear growth rate may be degenerate with modifications to baryon physics behavior.

Galaxies and galaxy clusters form in high-density, virialized regions defined by the dark matter halo population. To link the outputs of *N*-body simulations to observable quantities, a common approach is to derive empirical scaling relations between halo properties (typically mass or circular velocity) and an observable property of the halo (e.g. central galaxy luminosity or stellar mass, or cluster X-ray luminosity). An example of such an approach, the method of sub-halo abundance matching, has been shown to successfully reproduce the low-order clustering properties of galaxies observed over a wide range of redshifts [176,177]. Alternatively, one can trace a halo's growth history in a simulation and use that behavior, coupled with rules for internal baryon processing, to predict baryon properties over time. This so-called semi-analytic approach has seen good success, but increasingly complex models with large sets of control parameters are necessary to match a wide range of observations [178,179]. On the larger mass scales of galaxy clusters, one can also apply models for the hot gas distribution to predict observable X-ray and SZ signals [153].

N-body codes are largely mature. Comparisons of independent codes demonstrate percent-level agreement on the large-scale matter power spectrum [157] and the virial scaling (relation between velocity dispersion and mass) of dark matter halos [180]. Despite their mature status, *N*-body simulations will always be limited in their applicability to reality by the fact that baryons do not trace dark matter on strongly non-linear scales which, recall, *roughly* corresponds to scales of less than a few Mpc. Inclusion of realistic baryonic physics in cosmological simulations lies at the frontier of computational cosmology.

5.1.2. Hydrodynamical simulations

As mentioned in Section 4.3, there is rich dark energy information at small spatial scales, but one needs an accurate model for small-scale structure evolution in order to mine this territory productively. To model the growth of small-scale structure, it is essential to understand a multitude of baryonic processes, including radiative cooling, star and compact object formation, and feedback from supernovae and active galactic nuclei (AGN); see [181] for a recent review. This class of simulation is, in general, much more computationally intensive than *N*-body simulations, and the modeling of star formation and feedback processes is not yet well understood. For example, in high mass halos the central mass density profile can become more concentrated due to star formation or less concentrated by AGN feedback [182–186]. While initial studies of how baryonic processes alter the matter power spectrum [187–190] and the halo mass function [188,191,192] have been done, more work is needed to meaningfully constrain the small scale matter power spectrum and its evolution over cosmic time.

On very small scales, there have been several long-standing discrepancies between the structure predicted by ΛCDM and observational evidence, including the inner-slope of low-mass galaxy halos (cusp vs. core problem) and the number of satellite galaxies (missing satellite problem); see [55] for a recent review. It has recently been shown that the gravitational back-reaction on dark matter driven by small-scale baryonic feedback can solve these apparent discrepancies [193,194]. The largest halos are relatively immune to galaxy feedback, and early hydrodynamic simulations of purely gravitational evolution produced X-ray and SZ properties of the hot gas in galaxy clusters in reasonable agreement with observations [195]. Modern simulations are struggling to reproduce the low observed fraction of baryons that form stars, but AGN feedback mechanisms appear promising [181].

Hydrodynamical simulations produce smaller halo samples than dark matter simulations, so results are often limited by sample variance. Because of astrophysics uncertainties, relatively little attention has been paid to hydrodynamical simulations in modified gravity models or alternate dark energy models.

5.1.3. Synthetic skies

Synthetic galaxy catalogs based on *N*-body simulations are becoming an indispensable guide for science analysis of large-angle photometric and spectroscopic surveys [196–204]. Such catalogs provide truth tables that can be processed through selection machinery to generate survey-specific expectations. This process can help guide survey strategy and plan follow-up campaigns, as well as enable insights into sources of systematic errors in science analysis. Recent examples include covariance estimates for SDSS-III BOSS clustering analysis based on the synthetic catalogs of [205], and the support of galaxy group analysis in the WiggleZ spectroscopic survey from the GiggleZ simulations [206].

The increasing sensitivity and sky coverage of galaxy surveys will only increase the demand for high-fidelity, multi-wavelength synthetic sky maps. In particular, catalog-level expectations derived from a simple observational transfer function may be insufficient. The ultimate approach would incorporate the propagation and acquisition of source photons, and their subsequent conversion to detector signals.

5.2. Simulating a new generation of cosmological probes

The stringent requirements described above for the control of systematic errors and uncertainties within cosmological experiments necessitate a detailed understanding of the properties of individual experiments or surveys. Systematic effects can arise from the design of the system (e.g. ghosting of images or scatter light), from the response of the atmosphere (e.g. the stability of the point-spread-function or the variability in the transmissivity of the sky), from the strategy used to survey the sky (e.g. inhomogeneous sampling of astronomical light curves), or from limitations in an analysis algorithms (e.g. due to the finite processing power available for characterizing the properties of detected sources).

Understanding which of these issues will impact the science (and how) is critical if we hope to maximize our scientific returns.

Over the last few years, simulation frameworks have demonstrated that they can provide such a capability; delivering a virtual prototype against which design decisions, optimizations (including descoping), and trade studies can be evaluated [207]. What defines the range of capabilities and fidelity required for a simulation framework? There are clearly trade-offs between engineering tools, end-to-end simulators, and the use of extant data sets. Engineering simulations such as Zemax are typically used to define the optical design of the system. While detailed, these modeling tools do not couple to the astrophysical properties of the sky nor the variations in observing conditions. They are not designed to scale to the size of large scale experiments or surveys. Extant data sets, in contrast, provide a representative view of the complexity of observations and the Universe as a whole. They are, however, constrained by the fact that they represent an existing experiments and any inherent systematics might not reflect the design of a new experiment. For example, in the case of the LSST [208], the science requirements specify levels of accuracy in characterizing the photometric, astrometric and shape properties of stars and galaxies that are between a factor of two and one hundred times better than current surveys [209].

5.2.1. Design through simulation

Instrument simulators, coupled to models of the observable Universe and to simulations of the cadence of a survey (i.e. the time and positional dependence of a sequence of observations) can provide data with the expected characteristics of a survey well in advance of first light. Detailed simulations of the design of a telescope, its optics, or the performance of a camera or spectrograph can identify the need for new calibration and software development efforts early in the process, thus enabling a project to prioritize the development effort to match the science requirements drivers (and identify which science aspects of the survey were insensitive to these effects). A simulation framework provides the ability to take a high level requirement, which incorporates optical-mechanical, atmospheric, electronic, and software components together with the underlying astrophysical distributions of sources, and evaluate which systematics are most sensitive to individual components (i.e. assuming we can model the simulation components at the appropriate level of fidelity). A simulation framework can provide an end-to-end implementation of the full flow of photons and information to evaluate the ability to achieve the science requirements or a simplification of the flow of information to identify the sub-components and their contribution to the overall performance.

There are a number of historical instances whereby the design of a survey (including the analysis software) has impacted the ability of that system to achieve, in a timely fashion, its stated photometric and astrometric performance. For example, for the case of the SDSS, the photometric performance of this system achieved better than 2% photometric calibration across its survey volume. To achieve this level of fidelity required the identification and correction of a number of features impacting the photometric performance. It was recognized, three years after first light, that an accurate model for the point-spread-function of the SDSS telescope and its variation across the focal plane needed to be developed [210]. After five years, techniques for a global photometric solution for the SDSS photometry were implemented in order to obtain a 2% photometric calibration [211]. Simulations provide the capability to address many of these issues prior to operations.

5.2.2. Performance verification

During the preconstruction and construction phases of any experiment, prototype devices and subcomponents will be delivered together with laboratory data on the performance of these systems (e.g. the delivery of sensors with measured quantum efficiencies, defects, and noise characteristics). Evaluating the impact of these components, prior to the completion of construction, is a non-trivial task. Engineering models and simulations provide some of these capabilities (e.g. the use of FRED to evaluate integrated scattered light). Laboratory measurements to date have not been able to equate directly to the science capabilities as we must couple the performance of a device with the properties of astrophysical sources and our ability to measure the properties of sources to characterize and correct for any systematic effects. Nevertheless, laboratory-based simulations of astrophysical sources may play a role in the future, and some steps in that direction have recently been made [212].

5.2.3. Diagnostics and trade studies

Science requirements propagate into scientific analyses. For example, the photometric redshifts, which are relied upon by many cosmological probes, depend on deblending of sources, photometric zero points, and the implementation of model-based magnitudes. Typically the requirement on the photometric redshift performance captures only the final level of fidelity (e.g. the variance or fraction of outliers in the redshift relation). Simulations, where the input configurations can be controlled, in conjunction with observational data sets, provide the ability to quantify the sensitivity of these requirements to the input parametrization of the Universe and the properties of the site. Trade studies, such as the impact of available compute resources on the fidelity of the derived shape parameters, can be undertaken in controlled situations to define what governs the sensitivity of the system.

References

[1] A. Kim, N. Padmanabhan, G. Aldering, S. Allen, C. Baltay et al., Distance probes of dark energy. Available from: <arXiv:1309.5382[astro-ph.CO]>.

[2] A. Jenkins et al., Virgo Consortium Collaboration, Evolution of structure in cold dark matter universes, Astrophys. J. 499 (1998) 20. Available from: <arXiv:astro-ph/9709010[astro-ph]>.

[3] G. Dvali, G. Gabadadze, M. Porrati, 4-D gravity on a brane in 5-D Minkowski space, Phys. Lett. B485 (2000) 208–214. Available from: <arXiv:hep-th/0005016[hep-th]>.

[4] E.V. Linder, Exponential gravity, Phys. Rev. D 80 (12) (2009) 123528. Available from: <arXiv:0905.2962[astro-ph.CO]>.

[5] B. Jain, A. Joyce, R. Thompson, A. Upadhye, J. Battat et al., Novel probes of gravity and dark energy. Available from: <arXiv:1309.5389[astro-ph.CO]>.

[6] B. Jain, J. Khoury, Cosmological tests of gravity, Ann. Phys. 325 (2010) 1479–1516. Available from: <arXiv:1004.3294[astro-ph.CO]>.

[7] W. Hu, I. Sawicki, Models of f(R) cosmic acceleration that evade solar-system tests, Phys. Rev. D76 (2007) 064004. Available from: <arXiv:0705.1158[astro-ph]>.

[8] B. Jain, V. Vikram, J. Sakstein, Astrophysical tests of modified gravity: constraints from distance indicators in the nearby universe, Astrophys. J. 779 (2013) 39. Available from: <arXiv:1204.6044[astro-ph.CO]>.

[9] V. Vikram, A. Cabr, B. Jain, J. VanderPlas, Astrophysical tests of modified gravity: the morphology and kinematics of Dwarf galaxies, JCAP 1308 (2013) 020. Available from: <arXiv:1303.0295[astro-ph.CO]>.

[10] Y.-S. Song, H. Peiris, W. Hu, Cosmological constraints on f(R) acceleration models, Phys. Rev. D76 (2007) 063517. Available from: <arXiv:0706.2399[astro-ph]>.

[11] T. Giannantonio, M. Martinelli, A. Silvestri, A. Melchiorri, New constraints on parametrised modified gravity from correlations of the CMB with large scale structure, JCAP 1004 (2010) 030. Available from: <arXiv:0909.2045[astro-ph.CO]>.

[12] F. Schmidt, A. Vikhlinin, W. Hu, Cluster constraints on f(R) gravity, Phys. Rev. D80 (2009) 083505. Available from: <arXiv:0908.2457[astro-ph.CO]>.

[13] L. Lombriser, F. Schmidt, T. Baldauf, R. Mandelbaum, U. Seljak, et al., Cluster density profiles as a test of modified gravity, Phys. Rev. D85 (2012) 102001. Available from: <arXiv:1111.2020[astro-ph.CO]>.

[14] L. Wang, P.J. Steinhardt, Cluster abundance constraints for cosmological models with a time-varying, spatially inhomogeneous energy component with negative pressure, ApJ 508 (1998) 483–490. Available from: <arXiv:astro-ph/9804015>.

[15] E.V. Linder, Cosmic growth history and expansion history, Phys. Rev. D 72 (4) (2005) 043529. Available from: <arXiv:astro-ph/0507263>.

[16] E.V. Linder, R.N. Cahn, Parameterized beyond-Einstein growth, Astropart. Phys. 28 (2007) 481–488. Available from: <arXiv:astro-ph/0701317>.

[17] E.V. Linder, Extending the gravitational growth framework, Phys. Rev. D 79 (6) (2009) 063519. Available from: <arXiv:0901.0918[astro-ph.CO]>.
[18] E.V. Linder, Testing dark matter clustering with redshift space distortions, J. Cosmol. Astropart. Phys. 4 (2013) 31. Available from: <arXiv:1302.4754[astro-ph.CO]>.
[19] C. di Porto, L. Amendola, Observational constraints on the linear fluctuation growth rate, Phys. Rev. D 77 (8) (2008) 083508. Available from: <arXiv:0707.2686>.
[20] R.A. Battye, J.A. Pearson, Parametrizing dark sector perturbations via equations of state, Phys. Rev. D 88 (6) (2013) 061301. Available from: <arXiv:1306.1175[astro-ph.CO]>.
[21] T. Baker, P.G. Ferreira, C. Skordis, A fast route to modified gravitational growth, Phys. Rev. D89 (2014) 024026. Available from: <arXiv:1310.1086[astro-ph.CO]>.
[22] S.F. Daniel, E.V. Linder, Constraining cosmic expansion and gravity with galaxy redshift surveys, J. Cosmol. Astropart. Phys. 2 (2013) 7. Available from: <arXiv:1212.0009[astro-ph.CO]>.
[23] S. Asaba, C. Hikage, K. Koyama, G.-B. Zhao, A. Hojjati, et al., Principal component analysis of modified gravity using weak lensing and peculiar velocity measurements, JCAP 1308 (2013) 029. Available from: <arXiv:1306.2546[astro-ph.CO]>.
[24] R. Bean, M. Tangmatitham, Current constraints on the cosmic growth history, Phys. Rev. D81 (2010) 083534. Available from: <arXiv:1002.4197[astro-ph.CO]>.
[25] G.-B. Zhao, H. Li, E.V. Linder, K. Koyama, D.J. Bacon, X. Zhang, Testing Einstein gravity with cosmic growth and expansion, Phys. Rev. D 85 (12) (2012) 123546. Available from: <arXiv:1109.1846[astro-ph.CO]>.
[26] J.N. Dossett, M. Ishak, J. Moldenhauer, Testing general relativity at cosmological scales: implementation and parameter correlations, Phys. Rev. D84 (2011) 123001. Available from: <arXiv:1109.4583[astro-ph.CO]>.
[27] A. Silvestri, L. Pogosian, R.V. Buniy, Practical approach to cosmological perturbations in modified gravity, Phys. Rev. D 87 (10) (2013) 104015. Available from: <arXiv:1302.1193[astro-ph.CO]>.
[28] K.S. Dawson, Schlegel, et al., The baryon oscillation spectroscopic survey of SDSS-III, AJ 145 (2013) 10. Available from: <arXiv:1208.0022[astro-ph.CO]>.
[29] N. Kaiser, Clustering in real space and in redshift space, MNRAS 227 (July) (1987) 1.
[30] J.C. Jackson, A critique of Rees's theory of primordial gravitational radiation, MNRAS 156 (1972) 1P.
[31] W.J. Percival et al., 2dFGRS Collaboration, The 2dF galaxy redshift survey: spherical harmonics analysis of fluctuations in the final catalogue, Mon. Not. R. Astron. Soc. 353 (2004) 1201. Available from: <arXiv:astro-ph/0406513[astro-ph]>.
[32] L. Guzzo, M. Pierleoni, B. Meneux, E. Branchini, O.L. Fevre, et al., A test of the nature of cosmic acceleration using galaxy redshift distortions, Nature 451 (2008) 541–545. Available from: <arXiv:0802.1944[astro-ph]>.
[33] J. da Angela, T. Shanks, S. Croom, P. Weilbacher, R. Brunner, et al., The 2dF-SDSS LRG and QSO Survey: QSO clustering and the L-z degeneracy, Mon. Not. R. Astron. Soc. 383 (2008) 565–580. Available from: <arXiv:astro-ph/0612401[astro-ph]>.
[34] A. Cabre, E. Gaztanaga, Clustering of luminous red galaxies I: large scale redshift space distortions, Mon. Not. R. Astron. Soc. 393 (2009) 1183–1208. Available from: <arXiv:0807.2460[astro-ph]>.
[35] L. Samushia, W.J. Percival, A. Raccanelli, Interpreting large-scale redshift-space distortion measurements, Mon. Not. R. Astron. Soc. 420 (2012) 2102–2119. Available from: <arXiv:1102.1014[astro-ph.CO]>.
[36] A. Raccanelli, D. Bertacca, D. Pietrobon, F. Schmidt, L. Samushia et al., Testing gravity using large-scale redshift-space distortions. Available from: <arXiv:1207.0500[astro-ph.CO]>.
[37] C. Blake, S. Brough, M. Colless, C. Contreras, W. Couch, et al., The WiggleZ dark energy survey: the growth rate of cosmic structure since redshift $z = 0.9$, Mon. Not. R. Astron. Soc. 415 (2011) 2876. Available from: <arXiv:1104.2948[astro-ph.CO]>.
[38] B.A. Reid, L. Samushia, White, et al., The clustering of galaxies in the SDSS-III baryon oscillation spectroscopic survey: measurements of the growth of structure and expansion rate at $z = 0.57$ from anisotropic clustering, MNRAS 426 (Nov) (2012) 2719–2737. Available from: <arXiv:1203.6641[astro-ph.CO]>.
[39] L. Samushia, B.A. Reid, M. White, et al., The clustering of galaxies in the SDSS-III DR9 baryon oscillation spectroscopic survey: testing deviations from Λ and general relativity using anisotropic clustering of galaxies, MNRAS 429 (2013) 1514–1528. Available from: <arXiv:1206.5309[astro-ph.CO]>.
[40] C.P. Ahn et al., The ninth data release of the sloan digital sky survey: first spectroscopic data from the SDSS-III baryon oscillation spectroscopic survey, ApJ Suppl. 203 (Dec.) (2012) 21. Available from: <arXiv:1207.7137[astro-ph.IM]>.
[41] PFS Team Collaboration, R. Ellis et al., Extragalactic science and cosmology with the subaru prime focus spectrograph (PFS). Available from: <arXiv:1206.0737[astro-ph.CO]>.
[42] M. White, Y.-S. Song, W.J. Percival, Forecasting cosmological constraints from redshift surveys, MNRAS 397 (Aug) (2009) 1348–1354. Available from: <arXiv:0810.1518>.
[43] C. Alcock, B. Paczynski, An evolution free test for non-zero cosmological constant, Nature 281 (1979) 358–359.
[44] T. Matsubara, Y. Suto, Cosmological redshift distortion of correlation functions as a probe of the density parameter and the cosmological constant, Astrophys. J. 470 (1996) L1–L5. Available from: <arXiv:astro-ph/9604142[astro-ph]>.
[45] W. Ballinger, J. Peacock, A. Heavens, Measuring the cosmological constant with redshift surveys, Mon. Not. R. Astron. Soc. 282 (1996) 877–888. Available from: <arXiv:astro-ph/9605017[astro-ph]>.
[46] J. Kwan, G.F. Lewis, E.V. Linder, Mapping growth and gravity with robust redshift space distortions, Astrophys. J. 748 (2012) 78. Available from: <arXiv:1105.1194[astro-ph.CO]>.
[47] A.J. Ross et al., Ameliorating systematic uncertainties in the angular clustering of galaxies: a study using the SDSS-III, MNRAS 417 (2011) 1350–1373. Available from: <arXiv:1105.2320[astro-ph.CO]>.
[48] A.J. Ross, W.J. Percival, A.G. Sánchez, L. Samushia, et al., The clustering of galaxies in the SDSS-III baryon oscillation spectroscopic survey: analysis of potential systematics, MNRAS 424 (July) (2012) 564–590. Available from: <arXiv:1203.6499[astro-ph.CO]>.
[49] S. Boughn, R. Crittenden, A Correlation of the cosmic microwave sky with large scale structure, Nature 427 (2004) 45–47. Available from: <arXiv:astro-ph/0305001[astro-ph]>.
[50] T. Giannantonio, R. Scranton, R.G. Crittenden, R.C. Nichol, S.P. Boughn, et al., Combined analysis of the integrated Sachs–Wolfe effect and cosmological implications, Phys. Rev. D77 (2008) 123520. Available from: <arXiv:0801.4380[astro-ph]>.
[51] S. Ho, C. Hirata, N. Padmanabhan, U. Seljak, N. Bahcall, Correlation of CMB with large-scale structure: I. ISW tomography and cosmological implications, Phys. Rev. D78 (2008) 043519. Available from: <arXiv:0801.0642[astro-ph]>.
[52] W. Hu, R. Scranton, Measuring dark energy clustering with CMB-galaxy correlations, Phys. Rev. D70 (2004) 123002. Available from: <arXiv:astro-ph/0408456[astro-ph]>.
[53] J. Rhodes, S. Allen, B. Benson, T. Chang, R. de Putter et al., Exploiting cross correlations and joint analyses, Available from: <arXiv:1309.5388[astro-ph.CO]>.
[54] S.W. Allen, A.E. Evrard, A.B. Mantz, Cosmological parameters from observations of galaxy clusters, Ann. Rev. Astron. Astrophys. 49 (2011) 409–470. Available from: <arXiv:1103.4829[astro-ph.CO]>.
[55] D.H. Weinberg, M.J. Mortonson, D.J. Eisenstein, C. Hirata, A.G. Riess, et al., Observational probes of cosmic acceleration, Phys. Rep. 530 (2013) 87–255. Available from: <arXiv:1201.2434[astro-ph.CO]>.
[56] W.H. Press, P. Schechter, Formation of galaxies and clusters of galaxies by self-similar gravitational condensation, ApJ 187 (Feb) (1974) 425–438.
[57] A. Mantz, S.W. Allen, D. Rapetti, The observed growth of massive galaxy clusters – IV. Robust constraints on neutrino properties, MNRAS 406 (Aug) (2010) 1805–1814. Available from: <arXiv:0911.1788[astro-ph.CO]>.
[58] Z. Hou, C. Reichardt, K. Story, B. Follin, R. Keisler, et al., Constraints on cosmology from the cosmic microwave background power spectrum of the 2500-square degree SPT-SZ survey, Astrophys. J. 782 (2014) 74. Available from: <arXiv:1212.6267[astro-ph.CO]>.
[59] R. Burenin, Possible indication for non-zero neutrino mass and additional neutrino species from cosmological observations, Astron. Lett. 39 (2013) 357–366. Available from: <arXiv:1301.4791[astro-ph.CO]>.
[60] E. Rozo, E.S. Rykoff, J.G. Bartlett, A.E. Evrard, Cluster cosmology at a crossroads: neutrino masses. Available from: <arXiv:1302.5086[astro-ph.CO]>.
[61] D. Nagai, A. Vikhlinin, A.V. Kravtsov, Testing X-ray measurements of galaxy clusters with cosmological simulations, Astrophys. J. 655 (2007) 98–108. Available from: <arXiv:astro-ph/0609247[astro-ph]>.
[62] E.T. Lau, A.V. Kravtsov, D. Nagai, Residual gas motions in the intracluster medium and bias in hydrostatic measurements of mass profiles of clusters, Astrophys. J. 705 (2009) 1129–1138. Available from: <arXiv:0903.4895[astro-ph.CO]>.
[63] N. Battaglia, J. Bond, C. Pfrommer, J. Sievers, On the cluster physics of Sunyaev–Zel'dovich surveys. I: The influence of feedback, non-thermal pressure and cluster shapes on Y–M scaling relations, Astrophys. J. 758 (2012) 74. Available from: <arXiv:1109.3709[astro-ph.CO]>.
[64] E. Rasia, M. Meneghetti, R. Martino, S. Borgani, A. Bonafede, et al., Lensing and X-ray mass estimates of clusters (SIMULATION), New J. Phys. 14 (2012) 055018. Available from: <arXiv:1201.1569[astro-ph.CO]>.
[65] J. Nevalainen, L. David, M. Guainazzi, Cross-calibrating X-ray detectors with clusters of galaxies: an IACHEC study, A & A 523 (2010) A22. Available from: <arXiv:1008.2102[astro-ph.IM]>.
[66] M. Tsujimoto et al., Cross-calibration of the X-ray instruments onboard the Chandra, INTEGRAL, RXTE, Suzaku, Swift, and XMM-Newton observatories using G21.5-0.9, A & A 525 (2011) A25. Available from: <arXiv:1009.2812[astro-ph.HE]>.
[67] D.E. Applegate, A. von der Linden, P.L. Kelly, M.T. Allen, S.W. Allen, et al., Weighing the giants III: methods and measurements of accurate galaxy cluster weak-lensing masses, Mon. Not. R. Astron. Soc. 439 (2014) 48–72. Available from: <arXiv:1208.0605[astro-ph.CO]>.
[68] C. Heymans et al., The shear testing programme – I. Weak lensing analysis of simulated ground-based observations, MNRAS 368 (2006) 1323–1339. Available from: <arXiv:astro-ph/0506112>.
[69] R. Massey et al., The shear testing programme. 2: Factors affecting high-precision weak-lensing analyses, MNRAS 376 (2007) 13–38. Available from: <arXiv:astro-ph/0608643>.
[70] T.D. Kitching et al., Image analysis for cosmology: results from the GREAT10 galaxy challenge, MNRAS 423 (2012) 3163–3208. Available from: <arXiv:1202.5254[astro-ph.CO]>.

[71] T. Kitching, J. Rhodes, C. Heymans, R. Massey, Q. Liu et al., Image analysis for cosmology: shape measurement challenge review & results from the mapping dark matter challenge. Available from: <arXiv:1204.4096[astro-ph.CO]>.
[72] A. Vallinotto, S. Dodelson, P. Zhang, Magnification as a tool in weak lensing, Phys. Rev. D84 (2011) 103004. Available from: <arXiv:1009.5590[astro-ph.CO]>.
[73] E. Rozo, F. Schmidt, Weak lensing mass calibration with shear and magnification. Available from: <arXiv:1009.5735[astro-ph.CO]>.
[74] E.M. Huff, G.J. Graves, Magnificent magnification: exploiting the other half of the lensing signal, Astrophys. J. 780 (2014) L16. Available from: <arXiv:1111.1070[astro-ph.CO]>.
[75] F. Schmidt, A. Leauthaud, R. Massey, J. Rhodes, M.R. George, A.M. Koekemoer, A. Finoguenov, M. Tanaka, A detection of weak-lensing magnification using galaxy sizes and magnitudes, Astrophys. J. Lett. 744 (2012) L22. Available from: <arXiv:1111.3679[astro-ph.CO]>.
[76] J. Coupon, T. Broadhurst, K. Umetsu, Cluster lensing profiles derived from a redshift enhancement of magnified BOSS-survey galaxies, Astrophys. J. 772 (2013) 65. Available from: <arXiv:1303.6588[astro-ph.CO]>.
[77] A.P. Hearin, A.R. Zentner, Z. Ma, D. Huterer, A general study of the influence of catastrophic photometric redshift errors on cosmology with cosmic shear tomography, Astrophys. J. 720 (2010) 1351–1369. Available from: <arXiv:1002.3383[astro-ph.CO]>.
[78] C.E. Cunha, D. Huterer, M.T. Busha, R.H. Wechsler, Sample variance in photometric redshift calibration: cosmological biases and survey requirements, MNRAS 423 (June) (2012) 909–924. Available from: <arXiv:1109.5691[astro-ph.CO]>.
[79] D. Huterer, C.E. Cunha, W. Fang, Calibration errors unleashed: effects on cosmological parameters and requirements for large-scale structure surveys, MNRAS 432 (2013) 2945. Available from: <arXiv:1211.1015[astro-ph.CO]>.
[80] J. Newman, A. Abate, F. Abdalla, S. Allam, S. Allen et al., Spectroscopic needs for imaging dark energy experiments: photometric redshift training and calibration. Available from: <arXiv:1309.5384[astro-ph.CO]>.
[81] J.A. Newman, Calibrating redshift distributions beyond spectroscopic limits with cross-correlations, ApJ 684 (Sept) (2008) 88–101. Available from: <arXiv:0805.1409>.
[82] M. McQuinn, M. White, On using angular cross-correlations to determine source redshift distributions, Mon. Not. R. Astron. Soc. 433 (2013) 2857. Available from: <arXiv:1302.0857[astro-ph.CO]>.
[83] H.-Y. Wu, E. Rozo, R.H. Wechsler, Annealing a follow-up program: improvement of the dark energy figure of merit for optical galaxy cluster surveys, Astrophys. J. 713 (2010) 1207–1218. Available from: <arXiv:0907.2690[astro-ph.CO]>.
[84] M. Oguri, M. Takada, Combining cluster observables and stacked weak lensing to probe dark energy: self-calibration of systematic uncertainties, Phys. Rev. D83 (2011) 023008. Available from: <arXiv:1010.0744[astro-ph.CO]>.
[85] E. Rozo, E.S. Rykoff, J.G. Bartlett, and A.E. Evrard, A Comparative Study of Local Galaxy Clusters: I. Derived X-ray Observables, Available from: <arXiv:1204.6301[astro-ph.CO]>.
[86] C.E. Cunha, Cross-calibration of cluster mass-observables, Phys. Rev. D79 (2009) 063009. Available from: <arXiv:0812.0583[astro-ph]>.
[87] C. Cunha, D. Huterer, J.A. Frieman, Constraining dark energy with clusters: complementarity with other probes, Phys. Rev. D80 (2009) 063532. Available from: <arXiv:0904.1589[astro-ph.CO]>.
[88] J.A. Tyson, R.A. Wenk, F. Valdes, Detection of systematic gravitational lens galaxy image alignments – mapping dark matter in galaxy clusters, Astrophys. J. Lett. 349 (1990) L1–L4.
[89] T.G. Brainerd, R.D. Blandford, I. Smail, Measuring galaxy masses using galaxy–galaxy gravitational lensing, Astrophys. J. 466 (1996) 623. Available from: <arXiv:astro-ph/9503073>.
[90] J. Miralda-Escude, The correlation function of galaxy ellipticities produced by gravitational lensing, Astrophys. J. 380 (1991) 1–8.
[91] N. Kaiser, Weak gravitational lensing of distant galaxies, Astrophys. J. 388 (1992) 272.
[92] B. Jain, U. Seljak, Cosmological model predictions for weak lensing: linear and nonlinear regimes, Astrophys. J. 484 (1997) 560. Available from: <arXiv:astro-ph/9611077>.
[93] D.J. Bacon, A.R. Refregier, R.S. Ellis, Detection of weak gravitational lensing by large-scale structure, Mon. Not. R. Astron. Soc. 318 (2000) 625. Available from: <arXiv:astro-ph/0003008>.
[94] N. Kaiser, G. Wilson, G.A. Luppino, Large-scale cosmic shear measurements, 2000. Available from: <arXiv:astro-ph/0003338>.
[95] L. van Waerbeke et al., Detection of correlated galaxy ellipticities on CFHT data: first evidence for gravitational lensing by large-scale structures, Astron. Astrophys. 358 (2000) 30–44. Available from: <arXiv:astro-ph/0002500>.
[96] D.M. Wittman, J.A. Tyson, D. Kirkman, I. Dell'Antonio, G. Bernstein, Detection of weak gravitational lensing distortions of distant galaxies by cosmic dark matter at large scales, Nature 405 (2000) 143–149. Available from: <arXiv:astro-ph/0003014>.
[97] H. Hoekstra, H.K.C. Yee, M.D. Gladders, Constraints on Ω_m and σ_8 from Weak Lensing in Red-Sequence Cluster Survey Fields, ApJ 577 (2002) 595–603. Available from: <arXiv:astro-ph/0204295>.
[98] M. Jarvis, G.M. Bernstein, P. Fischer, D. Smith, B. Jain, J.A. Tyson, D. Wittman, Weak-lensing results from the 75 square degree cerro tololo inter-American observatory survey, AJ 125 (2003) 1014–1032.
[99] T. Hamana et al., Cosmic shear statistics in the Suprime-Cam 2.1 square degree field: constraints on Ω_m and σ_8, ApJ 597 (2003) 98–110. Available from: <arXiv:astro-ph/0210450>.
[100] L. Van Waerbeke, Y. Mellier, H. Hoekstra, Dealing with systematics in cosmic shear studies: new results from the VIRMOS-Descart survey, A & A 429 (2005) 75–84. Available from: <arXiv:astro-ph/0406468>.
[101] C. Heymans et al., Cosmological weak lensing with the HST GEMS survey, MNRAS 361 (July) (2005) 160–176. Available from: <arXiv:astro-ph/0411324>.
[102] R. Massey et al., COSMOS: three-dimensional weak lensing and the growth of structure, ApJ S. 172 (2007) 239–253. Available from: <arXiv:astro-ph/0701480>.
[103] T.D. Kitching, A.F. Heavens, A.N. Taylor, M.L. Brown, K. Meisenheimer, C. Wolf, M.E. Gray, D.J. Bacon, Cosmological constraints from COMBO-17 using 3D weak lensing, MNRAS 376 (2007) 771–778. Available from: <arXiv:astro-ph/0610284>.
[104] T. Schrabback et al., Evidence of the accelerated expansion of the Universe from weak lensing tomography with COSMOS, A & A 516 (2010) A63. Available from: <arXiv:0911.0053[astro-ph.CO]>.
[105] E.M. Huff, T. Eifler, C.M. Hirata, R. Mandelbaum, D. Schlegel, U. Seljak, Seeing in the dark – II. Cosmic shear in the sloan digital sky survey, 2011. Available from: <arXiv:1112.3143[astro-ph.CO]>.
[106] M.J. Jee, J.A. Tyson, M.D. Schneider, D. Wittman, S. Schmidt, S. Hilbert, Cosmic shear results from the deep lens survey. I. Joint constraints on Ω_M and σ_8 with a two-dimensional analysis, ApJ 765 (2013) 74. Available from: <arXiv:1210.2732[astro-ph.CO]>.
[107] C. Heymans et al., CFHTLenS tomographic weak lensing cosmological parameter constraints: mitigating the impact of intrinsic galaxy alignments, MNRAS 432 (2013) 2433–2453. Available from: <arXiv:1303.1808[astro-ph.CO]>.
[108] A. Refregier, Weak gravitational lensing by large scale structure, Annu. Rev. Astron. Astrophys. 41 (2003) 645–668. Available from: <arXiv:astro-ph/0307212[astro-ph]>.
[109] H. Hoekstra, B. Jain, Weak gravitational lensing and its cosmological applications, Annu. Rev. Nucl. Part. Sci. 58 (2008) 99–123. Available from: <arXiv:0805.0139[astro-ph]>.
[110] D. Huterer, Weak lensing, dark matter and dark energy, Gen. Relativ. Gravitation 42 (2010) 2177–2195. Available from: <arXiv:1001.1758[astro-ph.CO]>.
[111] D.H. Rudd, A.R. Zentner, A.V. Kravtsov, Effects of baryons and dissipation on the matter power spectrum, Astrophys. J. 672 (2008) 19–32. Available from: <arXiv:astro-ph/0703741[ASTRO-PH]>.
[112] X. Yang, J.M. Kratochvil, K. Huffenberger, Z. Haiman, M. May, Baryon impact on weak lensing peaks and power spectrum: low-bias statistics and self-calibration in future surveys, Phys. Rev. D87 (2013) 023511. Available from: <arXiv:1210.0608[astro-ph.CO]>.
[113] A.R. Zentner, E. Semboloni, S. Dodelson, T. Eifler, E. Krause, et al., Accounting for baryons in cosmological constraints from cosmic shear, Phys. Rev. D87 (4) (2013) 043509. Available from: <arXiv:1212.1177[astro-ph.CO]>.
[114] W. Hu, Power spectrum tomography with weak lensing, Astrophys. J. 522 (1999) L21–L24. Available from: <arXiv:astro-ph/9904153>.
[115] J. Frieman, M. Turner, D. Huterer, Dark energy and the accelerating universe, Annu. Rev. Astron. Astrophys. 46 (2008) 385–432. Available from: <arXiv:0803.0982[astro-ph]>.
[116] M. Jarvis, M. Takada, B. Jain, G. Bernstein, Weak lensing cosmology with LSST: three-point shear correlations, in: American Astronomical Society Meeting Abstracts, vol. 36, Bulletin of the American Astronomical Society, 2004, p. 108.17.
[117] J.M. Kratochvil, Z. Haiman, M. May, Probing cosmology with weak lensing peak counts, Phys. Rev. D81 (2010) 043519. Available from: <arXiv:0907.0486[astro-ph.CO]>.
[118] J.M. Kratochvil, E.A. Lim, S. Wang, Z. Haiman, M. May, et al., Probing cosmology with weak lensing Minkowski functionals, Phys. Rev. D85 (2012) 103513. Available from: <arXiv:1109.6334[astro-ph.CO]>.
[119] J.-P. Uzan, F. Bernardeau, Lensing at cosmological scales: a test of higher dimensional gravity, Phys. Rev. D64 (2001) 083004. Available from: <arXiv:hep-ph/0012011>.
[120] B. Jain, P. Zhang, Observational Tests of Modified Gravity, Phys. Rev. D78 (2008) 063503. Available from: <arXiv:0709.2375[astro-ph]>.
[121] E. Bertschinger, One gravitational potential or two? Forecasts and tests, Philos. Trans. R. Soc. Lond. A369 (2011) 4947–4961. Available from: <arXiv:1111.4659[astro-ph.CO]>.
[122] S. Bridle et al., Results of the GREAT08 challenge: an image analysis competition for cosmological lensing, MNRAS 405 (July) (2010) 2044–2061. Available from: <arXiv:0908.0945[astro-ph.CO]>.
[123] R. Mandelbaum, B. Rowe, J. Bosch, C. Chang, F. Courbin et al., The third gravitational lensing accuracy testing (GREAT3) challenge handbook. Available from: <arXiv:1308.4982[astro-ph.CO]>.
[124] Z.-M. Ma, W. Hu, D. Huterer, Effect of photometric redshift uncertainties on weak lensing tomography, Astrophys. J. 636 (2005) 21–29. Available from: <arXiv:astro-ph/0506614>.
[125] D. Huterer, M. Takada, Calibrating the nonlinear matter power spectrum: requirements for future weak lensing surveys, Astropart. Phys. 23 (2005) 369–376. Available from: <arXiv:astro-ph/0412142>.
[126] D.H. Rudd, A.R. Zentner, A.V. Kravtsov, Effects of baryons and dissipation on the matter power spectrum, Astrophys. J. 672 (2008) 19–32. Available from: <arXiv:astro-ph/0703741>.

[127] A.P. Hearin, A.R. Zentner, The influence of galaxy formation physics on weak lensing tests of general relativity, JCAP 0904 (2009) 032. Available from: <arXiv:0904.3334[astro-ph.CO]>.
[128] M. Takada, B. Jain, The impact of non-Gaussian errors on weak lensing surveys, Mon. Not. R. Astron. Soc. 395 (2009) 2065–2086. Available from: <arXiv:0810.4170[astro-ph]>.
[129] A. Taylor, B. Joachimi, T. Kitching, Putting the precision in precision cosmology: how accurate should your data covariance matrix be? Available from: <arXiv:1212.4359[astro-ph.CO]>.
[130] S. Dodelson, M.D. Schneider, The effect of covariance estimator error on cosmological parameter constraints, Phys. Rev. D88 (2013) 063537. Available from: <arXiv:1304.2593[astro-ph.CO]>.
[131] D. Huterer, M. Takada, G. Bernstein, B. Jain, Systematic errors in future weak lensing surveys: requirements and prospects for self-calibration, Mon. Not. R. Astron. Soc. 366 (2006) 101–114. Available from: <arXiv:astro-ph/0506030>.
[132] B. Joachimi, S.L. Bridle, Simultaneous measurement of cosmology and intrinsic alignments using joint cosmic shear and galaxy number density correlations, A & A 523 (2010) A1. Available from: <arXiv:0911.2454[astro-ph.CO]>.
[133] B. Joachimi, S. Bridle, Simultaneous measurement of cosmology and intrinsic alignments using joint cosmic shear and galaxy number density correlations, Astron. Astrophys. 523 (2010) A1. Available from: <arXiv:0911.2454[astro-ph.CO]>.
[134] D. Kirk, S. Bridle, M. Schneider, The impact of intrinsic alignments: cosmological constraints from a joint analysis of cosmic shear and galaxy survey data, Mon. Not. R. Astron.Soc. 408 (2010) 1502–1515. Available from: <arXiv:1001.3787[astro-ph.CO]>.
[135] I. Laszlo, R. Bean, D. Kirk, S. Bridle, Disentangling dark energy and cosmic tests of gravity from weak lensing systematics. Available from: <arXiv:1109.4535[astro-ph.CO]>.
[136] D. Kirk, I. Laszlo, S. Bridle, R. Bean, Optimising cosmic shear surveys to measure modifications to gravity on cosmic scales. Available from: <arXiv:1109.4536[astro-ph.CO]>.
[137] C.M. Hirata, R. Mandelbaum, M. Ishak, U. Seljak, R. Nichol, K.A. Pimbblet, N.P. Ross, D. Wake, Intrinsic galaxy alignments from the 2SLAQ and SDSS surveys: luminosity and redshift scalings and implications for weak lensing surveys, MNRAS 381 (2007) 1197–1218. Available from: <arXiv:astro-ph/0701671>.
[138] B. Joachimi, R. Mandelbaum, F.B. Abdalla, S.L. Bridle, Constraints on intrinsic alignment contamination of weak lensing surveys using the MegaZ-LRG sample, A & A 527 (2011) A26. Available from: <arXiv:1008.3491[astro-ph.CO]>.
[139] D. Hanson, A. Challinor, A. Lewis, Weak lensing of the CMB, Gen. Relativ. Gravitation 42 (2010) 2197–2218. Available from: <arXiv:0911.0612[astro-ph.CO]>.
[140] S. Das, T.A. Marriage, P.A. Ade, P. Aguirre, M. Amir, et al., The Atacama cosmology telescope: a measurement of the cosmic microwave background power spectrum at 148 and 218 GHz from the 2008 southern survey, Astrophys. J. 729 (2011) 62. Available from: <arXiv:1009.0847[astro-ph.CO]>.
[141] S. Das, T. Louis, M.R. Nolta, G.E. Addison, E.S. Battistelli, et al., The Atacama cosmology telescope: temperature and gravitational lensing power spectrum measurements from three seasons of data, JCAP 1404 (2014) 014. Available from: <arXiv:1301.1037[astro-ph.CO]>.
[142] A. van Engelen, R. Keisler, O. Zahn, K. Aird, B. Benson, et al., A measurement of gravitational lensing of the microwave background using south pole telescope data, Astrophys. J. 756 (2012) 142. Available from: <arXiv:1202.0546[astro-ph.CO]>.
[143] Planck Collaboration, P. Ade et al., Planck 2013 results. XVII. Gravitational lensing by large-scale structure. Available from: <arXiv:1303.5077[astro-ph.CO]>.
[144] M. Niemack, P. Ade, J. Aguirre, F. Barrientos, J. Beall, et al., ACTPol: a polarization-sensitive receiver for the Atacama cosmology telescope, Proc. SPIE Int. Soc. Opt. Eng. 7741 (2010) 77411S. Available from: <arXiv:1006.5049[astro-ph.IM]>.
[145] M. Doran, G. Robbers, Early dark energy cosmologies, JCAP 0606 (2006) 026. Available from: <arXiv:astro-ph/0601544[astro-ph]>.
[146] E. Calabrese, R. de Putter, D. Huterer, E.V. Linder, A. Melchiorri, Future CMB constraints on early, cold, or stressed dark energy, Phys. Rev. D 83 (2011) 023011. Available from: <arXiv:1010.5612[astro-ph.CO]>.
[147] D. Hanson et al., SPTpol Collaboration, Detection of B-mode polarization in the cosmic microwave background with data from the south pole telescope, Phys. Rev. Lett. 111 (14) (2013) 141301. Available from: <arXiv:1307.5830[astro-ph.CO]>.
[148] A. Vallinotto, Using CMB lensing to constrain the multiplicative bias of cosmic shear, Astrophys. J. 759 (2012) 32. Available from: <arXiv:1110.5339[astro-ph.CO]>.
[149] S. Das, J. Errard, D. Spergel, Can CMB lensing help cosmic shear surveys? Available from: <arXiv:1311.2338[astro-ph.CO]>.
[150] M. Kuhlen, M. Vogelsberger, R. Angulo, Numerical simulations of the dark universe: state of the art and the next decade, Phys. Dark Universe 1 (2012) 50–93. Available from: <arXiv:1209.5745[astro-ph.CO]>.
[151] J.-M. Alimi, V. Bouillot, Y. Rasera, V. Reverdy, P.-S. Corasaniti, I. Balmes, S. Requena, X. Delaruelle, J.-N. Richet, DEUS full observable ΛCDM universe simulation: the numerical challenge, 2012. Available from: <arXiv:1206.2838[astro-ph.CO]>.
[152] J. Kim, C. Park, G. Rossi, S.M. Lee, J.R. Gott III, The new horizon run cosmological *N*-body simulations, J. Korean Astron. Soc. 44 (2011) 217–234. Available from: <arXiv:1112.1754[astro-ph.CO]>.
[153] R.E. Angulo, V. Springel, S.D.M. White, A. Jenkins, C.M. Baugh, C.S. Frenk, Scaling relations for galaxy clusters in the millennium-XXL simulation, Mon. Not. R. Astron. Soc. 426 (2012) 2046–2062. Available from: <arXiv:1203.3216[astro-ph.CO]>.
[154] S. Habib, V. Morozov, H. Finkel, A. Pope, K. Heitmann, K. Kumaran, T. Peterka, J. Insley, D. Daniel, P. Fasel, N. Frontiere, Z. Lukic, The universe at extreme scale: multi-petaflop sky simulation on the BG/Q, 2012. Available from: <arXiv:1211.4864[cs.DC]>.
[155] T. Ishiyama, K. Nitadori, J. Makino, 4.45 Pflops astrophysical N-body simulation on K computer – the gravitational trillion-body problem, 2012. Available from: <arXiv:1211.4406[astro-ph.CO]>.
[156] J. Carlson, M. White, N. Padmanabhan, Critical look at cosmological perturbation theory techniques, Phys. Rev. D 80 (2009) 043531. Available from: <arXiv:0905.0479[astro-ph.CO]>.
[157] K. Heitmann, M. White, C. Wagner, S. Habib, D. Higdon, The coyote universe. I. Precision determination of the nonlinear matter power spectrum, ApJ 715 (2010) 104–121. Available from: <arXiv:0812.1052>.
[158] R.K. Sheth, G. Tormen, Large-scale bias and the peak background split, MNRAS 308 (1999) 119–126.
[159] A. Jenkins, C.S. Frenk, S.D.M. White, J.M. Colberg, S. Cole, A.E. Evrard, H.M.P. Couchman, N. Yoshida, The mass function of dark matter haloes, MNRAS 321 (2001) 372–384. Available from: <arXiv:astro-ph/0005260>.
[160] D. Reed, J. Gardner, T. Quinn, J. Stadel, M. Fardal, G. Lake, F. Governato, Evolution of the mass function of dark matter haloes, MNRAS 346 (2003) 565–572. Available from: <arXiv:astro-ph/0301270>.
[161] Z. Lukić, K. Heitmann, S. Habib, S. Bashinsky, P.M. Ricker, The Halo mass function: high-redshift evolution and universality, ApJ 671 (2007) 1160–1181. Available from: <arXiv:astro-ph/0702360>.
[162] J. Tinker, A.V. Kravtsov, A. Klypin, K. Abazajian, M. Warren, G. Yepes, S. Gottlöber, D.E. Holz, Toward a Halo mass function for precision cosmology: the limits of universality, ApJ 688 (2008) 709–728. Available from: <arXiv:0803.2706>.
[163] M. Crocce, P. Fosalba, F.J. Castander, E. Gaztañaga, Simulating the Universe with MICE: the abundance of massive clusters, MNRAS (2010) 198. Available from: <arXiv:0907.0019>.
[164] C.E. Cunha, A.E. Evrard, Sensitivity of galaxy cluster dark energy constraints to halo modeling uncertainties, Phys. Rev. D 81 (2010) 083509. Available from: <arXiv:0908.0526[astro-ph.CO]>.
[165] H.-Y. Wu, A.R. Zentner, R.H. Wechsler, The impact of theoretical uncertainties in the Halo mass function and Halo bias on precision cosmology, ApJ 713 (Apr) (2010) 856–864. Available from: <arXiv:0910.3668[astro-ph.CO]>.
[166] J.-M. Alimi, A. Fuzfa, V. Boucher, Y. Rasera, J. Courtin, et al., Imprints of dark energy on cosmic structure formation. I. Realistic quintessence models, Mon. Not. R. Astron. Soc. 401 (2010) 775. Available from: <arXiv:0903.5490[astro-ph.CO]>.
[167] S. Bhattacharya, K. Heitmann, M. White, Z. Lukic, C. Wagner, et al., Mass function predictions beyond LCDM, Astrophys. J. 732 (2011) 122. Available from: <arXiv:1005.2239[astro-ph.CO]>.
[168] H. Oyaizu, Nonlinear evolution of f(R) cosmologies. I. Methodology, Phys. Rev. D 78 (12 Dec) (2008) 123523. Available from: <arXiv:0807.2449>.
[169] F. Schmidt, M. Lima, H. Oyaizu, W. Hu, Nonlinear evolution of f(R) cosmologies. III. Halo statistics, Phys. Rev. D 79 (8) (2009) 083518. Available from: <arXiv:0812.0545>.
[170] K.C. Chan, R. Scoccimarro, Large-scale structure in brane-induced gravity. II. Numerical simulations, Phys. Rev. D 80 (10) (2009) 104005. Available from: <arXiv:0906.4548[astro-ph.CO]>.
[171] J. Khoury, M. Wyman, *N*-body simulations of DGP and degravitation theories, Phys. Rev. D 80 (6) (2009) 064023. Available from: <arXiv:0903.1292[astro-ph.CO]>.
[172] B. Li, G.-B. Zhao, R. Teyssier, K. Koyama, ECOSMOG: an efficient code for simulating modified gravity, JCAP 1 (Jan) (2012) 51. Available from: <arXiv:1110.1379[astro-ph.CO]>.
[173] M. Baldi, V. Pettorino, G. Robbers, V. Springel, Hydrodynamical *N*-body simulations of coupled dark energy cosmologies, MNRAS 403 (Apr) (2010) 1684–1702. Available from: <arXiv:0812.3901>.
[174] W. Cui, M. Baldi, S. Borgani, The Halo mass function in interacting dark energy models, MNRAS 424 (Aug) (2012) 993–1005. Available from: <arXiv:1201.3568[astro-ph.CO]>.
[175] J. Koda, P.R. Shapiro, Gravothermal collapse of isolated self-interacting dark matter haloes: *N*-body simulation versus the fluid model, MNRAS 415 (Aug) (2011) 1125–1137. Available from: <arXiv:1101.3097[astro-ph.CO]>.
[176] C. Conroy, R.H. Wechsler, A.V. Kravtsov, Modeling luminosity-dependent galaxy clustering through cosmic time, ApJ 647 (2006) 201–214. Available from: <arXiv:astro-ph/0512234>.
[177] R.M. Reddick, R.H. Wechsler, J.L. Tinker, P.S. Behroozi, The connection between galaxies and dark matter structures in the local universe, Astrophys. J. 771 (2013) 30. Available from: <arXiv:1207.2160[astro-ph.CO]>.
[178] C.M. Baugh, A primer on hierarchical galaxy formation: the semi-analytical approach, Rep. Prog. Phys. 69 (2006) 3101–3156. Available from: <arXiv:astro-ph/0610031[astro-ph]>.
[179] A.J. Benson, Galaxy formation theory, Phys. Rep. 495 (Oct) (2010) 33–86. Available from: <arXiv:1006.5394[astro-ph.CO]>.

[180] A.E. Evrard et al., Virial scaling of massive dark matter halos: why clusters prefer a high normalization cosmology, ApJ 672 (2008) 122–137. Available from: <arXiv:astro-ph/0702241>.
[181] S. Borgani, A. Kravtsov, Cosmological simulations of galaxy clusters, Adv. Sci. Lett. 4 (2011) 204–227.
[182] O.Y. Gnedin, A.V. Kravtsov, A.A. Klypin, D. Nagai, Response of dark matter Halos to condensation of baryons: cosmological simulations and improved adiabatic contraction model, ApJ 616 (2004) 16–26. Available from: <arXiv:astro-ph/0406247>.
[183] E. Rasia, G. Tormen, L. Moscardini, A dynamical model for the distribution of dark matter and gas in galaxy clusters, MNRAS 351 (2004) 237–252. Available from: <arXiv:astro-ph/0309405>.
[184] P.B. Tissera, S.D.M. White, S. Pedrosa, C. Scannapieco, Dark matter response to galaxy formation, MNRAS 406 (2010) 922–935. Available from: <arXiv:0911.2316[astro-ph.CO]>.
[185] D. Martizzi, R. Teyssier, B. Moore, T. Wentz, The effects of baryon, physics, black holes and active galactic nucleus feedback on the mass distribution in clusters of galaxies, MNRAS 422 (2012) 3081–3091. Available from: <arXiv:1112.2752[astro-ph.CO]>.
[186] A.B. Newman, T. Treu, R.S. Ellis, D.J. Sand, C. Nipoti, J. Richard, E. Jullo, The density profiles of massive, relaxed galaxy clusters. I. The total density over three decades in radius, ApJ 765 (2013) 24. Available from: <arXiv:1209.1391[astro-ph.CO]>.
[187] Y. Jing, Y. Suto, H. Mo, The dependence of dark Halo clustering on the formation epoch and the concentration parameter, Astrophys. J. 657 (2007) 664–668. Available from: <arXiv:astro-ph/0610099[astro-ph]>.
[188] D.H. Rudd, A.R. Zentner, A.V. Kravtsov, Effects of baryons and dissipation on the matter power spectrum, ApJ 672 (2008) 19–32. Available from: <arXiv:astro-ph/0703741>.
[189] M.P. van Daalen, J. Schaye, C. Booth, C.D. Vecchia, The effects of galaxy formation on the matter power spectrum: a challenge for precision cosmology, Mon. Not. R. Astron. Soc. 415 (2011) 3649–3665. Available from: <arXiv:1104.1174[astro-ph.CO]>.
[190] L. Casarini, S.A. Bonometto, S. Borgani, K. Dolag, G. Murante et al., Tomographic weak lensing shear spectra from large *N*-body and hydrodynamical simulations. Available from: <arXiv:1203.5251[astro-ph.CO]>.
[191] R. Stanek, D. Rudd, A.E. Evrard, The effect of gas physics on the Halo mass function, Mon. Not. R. Astron. Soc. 394 (2009) L11–L15. Available from: <arXiv:0809.2805>.
[192] W. Cui, S. Borgani, K. Dolag, G. Murante, L. Tornatore, The effects of baryons on the Halo mass function, MNRAS 423 (July) (2012) 2279–2287. Available from: <arXiv:1111.3066[astro-ph.CO]>.
[193] F. Governato, A. Zolotov, A. Pontzen, C. Christensen, S.H. Oh, A.M. Brooks, T. Quinn, S. Shen, J. Wadsley, Cuspy no more: how outflows affect the central dark matter and baryon distribution in Λ cold dark matter galaxies, MNRAS 422 (2012) 1231–1240. Available from: <arXiv:1202.0554[astro-ph.CO]>.
[194] R. Teyssier, A. Pontzen, Y. Dubois, J.I. Read, Cusp-core transformations in dwarf galaxies: observational predictions, MNRAS 429 (2013) 3068–3078. Available from: <arXiv:1206.4895[astro-ph.CO]>.
[195] A.E. Evrard, Formation and evolution of X-ray clusters – a hydrodynamic simulation of the intracluster medium, ApJ 363 (1990) 349–366.
[196] A.E. Evrard et al., Galaxy clusters in hubble volume simulations: cosmological constraints from sky survey populations, ApJ 573 (2002) 7–36. Available from: <arXiv:astro-ph/0110246>.
[197] V.R. Eke et al., Galaxy groups in the 2dFGRS: the group-finding algorithm and the 2PIGG catalogue, MNRAS 348 (2004) 866–878. Available from: <arXiv:astro-ph/0402567>.
[198] R. Yan, M. White, A.L. Coil, Mock catalogs for the DEEP2 redshift survey, ApJ 607 (2004) 739–750. Available from: <arXiv:astro-ph/0311230>.
[199] A. Balaguera-Antolínez, A.G. Sánchez, H. Böhringer, C. Collins, Constructing mock catalogues for the REFLEX II galaxy cluster sample, MNRAS 425 (2012) 2244–2254. Available from: <arXiv:1207.2138[astro-ph.CO]>.
[200] A. Font-Ribera, P. McDonald, J. Miralda-Escudé, Generating mock data sets for large-scale Lyman-α forest correlation measurements, J. Cosmology Astropart. Phys. 1 (2012) 1. Available from: <arXiv:1108.5606[astro-ph.CO]>.
[201] T. Sousbie, H. Courtois, G. Bryan, J. Devriendt, MoLUSC: a mock local universe survey constructor, ApJ 678 (2008) 569–577.
[202] B.F. Gerke, R.H. Wechsler, P.S. Behroozi, M.C. Cooper, R. Yan, et al., Improved mock galaxy catalogs for the DEEP2 galaxy redshift survey from subhalo abundance and environment matching, Astrophys. J. Suppl. 208 (2013) 1. Available from: <arXiv:1207.2214[astro-ph.CO]>.
[203] A.I. Merson et al., Lightcone mock catalogues from semi-analytic models of galaxy formation – I. Construction and application to the BzK colour selection, MNRAS 429 (2013) 556–578. Available from: <arXiv:1206.4049[astro-ph.CO]>.
[204] Y.-C. Cai, R.E. Angulo, C.M. Baugh, S. Cole, C.S. Frenk, A. Jenkins, Mock galaxy redshift catalogues from simulations: implications for Pan-STARRS1, MNRAS 395 (2009) 1185–1203. Available from: <arXiv:0810.2300>.
[205] M. Manera et al., The clustering of galaxies in the SDSS-III baryon oscillation spectroscopic survey: a large sample of mock galaxy catalogues, MNRAS 428 (2013) 1036–1054. Available from: <arXiv:1203.6609[astro-ph.CO]>.
[206] D. Parkinson et al., The WiggleZ dark energy survey: final data release and cosmological results, Phys. Rev. D 86 (10) (2012) 103518. Available from: <arXiv:1210.2130[astro-ph.CO]>.
[207] A.J. Connolly, The LSST Science Collaboration, Simulating the LSST system. <http://dx.doi.org/10.1117/12.857819>.
[208] LSST Collaboration, Z. Ivezic, J. Tyson, R. Allsman, J. Andrew, R. Angel, LSST: from science drivers to reference design and anticipated data products. Available from: <arXiv:0805.2366[astro-ph]>.
[209] Z. Ivezic, The LSST Science Collaboration, Large synoptic survey telescope (LSST) science requirements document. <http://www.lsst.org/files/docs/SRD.pdf>.
[210] Z. Ivezic et al., SDSS Collaboration, SDSS data management and photometric quality assessment, Astron. Nachr. 325 (2004) 583–589. Available from: <arXiv:astro-ph/0410195[astro-ph]>.
[211] N. Padmanabhan, D. Schlegel, D. Finkbeiner, J. Barentine, M. Blanton, et al., An improved photometric calibration of the sloan digital sky survey imaging data, Astrophys. J. 674 (2008) 1217–1233. Available from: <arXiv:astro-ph/0703454[ASTRO-PH]>.
[212] S. Seshadri, C. Shapiro, T. Goodsall, J. Fucik, C.M. Hirata et al., Initial results from a laboratory emulation of weak gravitational lensing measurements. Available from: <arXiv:1308.3875[astro-ph.IM]>.